Sediment Transport by Currents Plus Irregular Waves

M C Ockenden
R L Soulsby

Report SR 376
February 1994

HR Wallingford

Registered Office: **HR Wallingford Ltd.** Howbery Park, Wallingford, Oxfordshire, OX10 8BA, UK
Telephone: 0491 835381 International + 44 491 835381 Telex: 848552 HRSWAL G.
Facsimile: 0491 832233 International + 44 491 832233 Registered in England No. 2562099
HR Wallingford Ltd is a wholly owned subsidiary of HR Wallingford Group Ltd.

Contract

This report describes work funded by the Ministry of Agriculture, Fisheries and Food under Contract Number CSA 2089, for which the nominated officer was Mr B D Richardson and the HR Wallingford (HR) nominated officer was Dr W R White. Allied work funded by the Commission of the European Communities Directorate General for Science, Research and Development under Contract Number MAS2-CT92-0027, forming part of the MAST G8M Coastal Morphodynamics community research programme, is reported here as well. The HR job numbers were IAS 10 (MAFF) and IAS 164 (MAST G8M). This report is published on behalf of the Ministry of Agriculture, Fisheries and Food, but any opinions expressed in this report are not necessarily those of the funding Ministry. The work was carried out by Ms M C Ockenden and R L Soulsby and the project was managed by R L Soulsby.

Prepared by M. C. Ockenden (name) PROJECT OFFICER (Job title)

Approved by R L. Soulsby Project Manager

Date 28. 2. 94

Summary

Sediment Transport by Currents Plus Irregular Waves

M C Ockenden
R L Soulsby

Report SR 376
February 1994

Predictions of coastal evolution rely on sediment transport formulae, but these are usually given only for the idealised case of currents combined with monochromatic, unidirectional waves. This report addresses the problem of making sediment transport predictions for the case of currents plus an irregular, multidirectional spectrum of waves as found in the real sea.

The optimal choice of wave friction factor, and a methodology for predicting the bed shear-stress time-series for irregular waves plus currents, are devised. These are applied to a large number of data-sets of bottom velocity, some of which are simulated and some taken from field measurements, and the resulting bed shear-stresses used in a sediment transport formula to predict the mean sediment transport rate for each data-set.

Although strictly it is impossible to find an equivalent regular wave which produces the same mean transport rate as the full irregular wave (because the regular wave has a very different probability distribution of bed shear-stress), it is nevertheless shown to be possible to specify an equivalent regular wave which gives the same mean sediment transport rate as the irregular wave to within ±20% for most cases.

The equivalent regular wave is shown to be specified by a bottom orbital velocity amplitude equal to $\sqrt{2}$ times the root-mean-square of the bottom velocity fluctuation of the irregular wave, a period equal to its peak period, and a direction equal to the mean direction of the wave spectrum. The tests covered a wide variety of current speeds; wave heights, periods, directions relative to current, spectral forms, and directional spreadings; and sediment grain sizes. Although these results were derived only for bedload transport, similar methods could be applied for suspended sediment transport.

This unrestricted report describes original research intended for use by hydraulic and coastal engineering consultants. Further information is available from R L Soulsby, head of the Marine Sediments Group.

Contents

Contents *continued*

Tables

Figures

Contents continued

1 Introduction

1.1 Objectives

A wide variety of coastal problems rely on accurate prediction of sediment transport in response to the action of waves and currents. However, prediction of the effect of waves on sediment transport is still generally restricted to monochromatic, unidirectional, non-breaking waves. In real sea conditions, where an irregular, directional spectrum of waves is encountered, the non-linear process of sediment transport may respond in a rather different way to the idealised regular wave case. Other aspects such as wave-breaking and wave asymmetry are also important in terms of sediment transport, particularly in shallow water as in the coastal environment.

The physical processes of sediment transport under irregular waves have been addressed in a two-year study commissioned by MAFF, starting in December 1991. This report covers only one part of this study. The objective of this part of the study was:

- to develop techniques for applying the presently available sediment transport predictors (for monochromatic, unidirectional waves) to the real conditions of an irregular, directional spectrum of waves.

As an alternative to running a full wave boundary layer numerical model, this study looked for a simple way to predict the mean sediment transport under irregular waves and currents from a small number of readily available parameters (such as spectrum shape, significant wave height, H_s, wave period, T_p, at the peak of the spectrum and angle of waves relative to the current). The method was tested by comparing the transport under the irregular wave spectrum with the transport calculated for an "equivalent" regular wave. An "equivalent" regular wave was defined as one which gave approximately the same sediment transport rate as the irregular wave spectrum or could be scaled by a constant factor to give the same transport rate.

1.2 Background

The numerical modelling of sediment transport in coastal areas has developed rapidly in recent years. Much effort has been put into understanding the hydrodynamics of combined wave and current flows, with the development of many boundary layer models for calculating the bottom friction effects. Some of these models have been compared in an inter-comparison exercise within the EC funded MAST G6M Coastal Morphodynamics programme, from which a parametrisation of the mean bed shear stress and maximum bed shear stress was derived (Soulsby et al., 1993). However, all the currently available models assume that waves are monochromatic and unidirectional, which is certainly not the case in real seas.

There have been studies to look at energy dissipation rates under a spectrum of waves (eg. Brampton et al., 1984; Madsen et al., 1988), but these were not extended to look at the sediment transport. A recent study by Zhao and Anastasiou (1993) parameterised the bottom friction effects under an irregular wave spectrum, but this was all based on a combined current and wave velocity at "Bijker's point" which is very close to the bed (= ez_0 above the bed). In terms of sediment transport, this is virtually within the layer of sediment grains at the surface.

Zyserman and Fredsøe (1988) carried out a study with similar aims to this one, in that they sought to define the characteristics of a regular wave which would give the same sediment transport as a spectrum of irregular waves. Their study addressed transport of the suspended sediment. It is based on "synthetic" wave data, ie the bottom orbital velocities were generated from the parameters defining the wave spectrum. Linear wave theory was used in this transformation. A boundary layer model (Fredsøe, 1984) was used to calculate the shear stresses. The study concluded that a sinusoidal wave having a height H_{rms} and a period T_s (determined from the spectrum of irregular waves) gave a good representation of the amount of suspended sediment transported by irregular waves.

The present study aimed to extend the work of Zyserman and Fredsøe by using observed velocity data to calculate sediment transport rates, and using a simplified approach to calculating shear stresses. A much greater range of input conditions was used than used by Zyserman and Fredsøe, giving greater information about sensitivity to aspects such as directional spreading and spectral width, and greater confidence in the method.

2 Method of approach

To parameterise the sediment transport in terms of the wave spectrum and a few other parameters, it is necessary to start from the surface elevation spectrum which must be transformed into orbital velocities at the bed and then to bed shear stress. The bed shear stress is used in a sediment transport formula. This route from surface elevation to sediment transport is shown in Figure 1. It was followed in this study for both the irregular waves and the corresponding regular waves. The ratio of the mean transport under irregular waves to the mean transport under regular waves was calculated.

The regular wave was chosen to be a unidirectional sine wave with orbital velocity amplitude = $\sqrt{2}U_{rms}$, period T_p, and direction equal to the mean direction of the irregular waves, where U_{rms} is the root-mean-square of the bottom orbital velocities in the irregular wave spectrum and T_p is the wave period at the peak of the spectrum. This is approximately equivalent to the wave of height H_{rms} and period T_s which Zyserman and Fredsøe found to give the best representation of the irregular wave.

The problem is highly nonlinear; at three points in the process it is necessary to make nonlinear transformations (Figure 1). If this were not so, it would be straightforward to move from the regular to the irregular wave case. The importance of the nonlinearity is therefore central to this study.

In transforming from a surface elevation spectrum or time series to orbital velocities at the bed, the usual method is to make linear wave theory assumptions. This does not allow for the asymmetry of the waves between crests and troughs which occurs as a result of nonlinear processes. By concentrating mainly on field data of observed time series of bottom orbital velocity, this study avoids the need to make the linear wave theory assumptions, since any asymmetry of the waves should be seen in the recorded bottom orbital velocities. However, in order to test the method over a wider range of variables and to test the sensitivity of the variables some simulated wave data was used, in which linear theory was used in the transformation from surface elevation to bottom orbital velocity.

The field data were collected in previous studies using STABLE (Sediment Transport And Boundary Layer Equipment). Deployments were made by the Proudman Oceanographic Laboratory off the south west coast of the Isle of Wight (IOW) in 1986 (Soulsby and Humphery, 1989) and over Norfolk Sand Banks (NSB) in 1988 (HR Wallingford, 1991). STABLE is a self-recording frame which sits on the sea bed and records mean, turbulent and wave-induced velocities near the bed in combined wave and current flows.

It was decided to calculate only the bed load transport using this method, as no simple sediment transport formula for suspended load transport was available. An extension of this work to include suspended load transport via a full boundary-layer model is being undertaken in an allied MAFF-funded project by Dr A G Davies of Bangor University.

3 *Calculation of bed shear stress*

3.1 Waves only

3.1.1 Comparison of 'linearised' shear stress with 'quadratic' shear stress

One of the main difficulties in calculating sediment transport lies in the calculation of bed shear stress from wave and current velocities. As a first approximation, a linearised form of the shear stress was investigated. If waves only are considered, the instantaneous shear stress, $\tau(t)$, can be expressed as a quadratic function of the velocity, ie

$$\underset{\sim}{\tau}(t) = \frac{1}{2}\rho f_w \underset{\sim}{u}(t)\,|\underset{\sim}{u}(t)| \qquad (1)$$

where

$\underset{\sim}{\tau}(t)$	is the instantaneous shear stress vector
ρ	is the water density
f_w	is the wave friction factor
$\underset{\sim}{u}(t)$	is the instantaneous velocity vector

The direction of the instantaneous shear stress is assumed to be the same as the instantaneous velocity, and the phase shift between u(t) and $\tau(t)$ is ignored in Equation 1.

A linearised form of this is

$$\underset{\sim}{\tau}(t) = \frac{1}{2}\rho f_w \underset{\sim}{u}(t)\,U_{rms} \qquad (2)$$

where

U_{rms} is the root-mean-square of the complete velocity record.

If a constant wave friction factor is assumed, then the ratio of the "full" shear stress to the linearised shear stress at any time becomes

$$\frac{\underset{\sim}{\tau}(t)_{full}}{\underset{\sim}{\tau}(t)_{linear}} = \frac{|\underset{\sim}{u}(t)|}{U_{rms}} \tag{3}$$

Using simulated wave data, the percentage exceedence curves for this ratio were calculated. These are shown in Figure 2 for both a spectrum with uni-directional waves and a spectrum with a cosine-squared spreading function. As U_{rms} is constant for a particular record, the percentage exceedence for u(t) reflects the distribution of the velocity. The uni-directional spectrum conforms almost exactly to the percentage exceedence for a Gaussian distribution, with approximately 32% of the distribution greater than one standard deviation from the mean. The multi-directional spectrum has a slightly different distribution but is fairly similar to the Gaussian distribution.

The distribution of velocities was checked using observed data collected from the STABLE deployment off the Isle of Wight. Bursts of data (approximately 8 minutes) were chosen in which there was very little mean current and nearly all the velocity fluctuation could be attributed to wave activity. An example is shown in Figure 3, in which the top figure shows the scatter plot of the velocities for burst 25 and the lower figure shows the percentage exceedence curve for the ratio of u(t) to U_{rms} (where u(t) is the velocity fluctuation once the mean current has been removed). The ratio also follows a Gaussian curve very closely, and it can be seen that for a small percentage of the time u(t) exceeds U_{rms} by a factor of two or three. As these large waves may be the ones responsible for a proportionately large amount of the sediment transport, it was decided that the linearised form of the shear stress was an inadequate approximation for the purposes of sediment transport.

Figure 4 shows the percentage exceedence curve for three bursts from the Isle of Wight, along with the Gaussian curve and the exceedence curve for the synthetic multidirectional spectrum. The data from the Isle of Wight falls between these two curves.

3.1.2 Choice of wave friction factor for a wave spectrum

The wave friction factor, f_w, is usually defined as a function of the wave excursion length, A, and the bottom roughness, z_0. Calculations are sometimes based on the Swart formula (Swart, 1974):

$$\begin{aligned} f_w &= 0.00251\ \exp\left(5.21\left(\frac{A}{k_s}\right)^{-0.19}\right), && \text{for } A/k_s > 1.57 \\ f_w &= 0.3 \qquad\qquad\qquad\qquad\quad , && \text{for } A/k_s \leq 1.57 \end{aligned} \tag{4}$$

where k_s is the Nikuradse roughness, normally taken to be equivalent to $30z_0$.

A simpler power law, which gives a better fit to data, is proposed by Soulsby (1993):

$$f_w = 1.39\left(\frac{A}{z_0}\right)^{-0.52} \tag{5}$$

In both cases, A is the (constant) wave excursion amplitude for a regular wave. The curves for both formulae are shown on Figure 5. This raises the question of whether a constant wave friction factor still applies when the waves form a whole spectrum.

According to Tucker (1991), if the distribution of the time series of surface elevation forms a narrow-banded Gaussian distribution then the distribution of maximum wave heights will be a Rayleigh distribution. The probability of a randomly chosen value of wave height falling between H-dH/2 and H+dH/2 is p(H)dH where

$$p(H) = \left(\frac{2H}{H_R^2}\right)\exp\left(\frac{-H^2}{H_R^2}\right) \qquad (6)$$

and

H_R = rms of the distribution of H

By analogy, since the distribution of the bottom orbital velocity u(t) is Gaussian, the distribution of maximum bottom orbital velocity should be a Rayleigh distribution.

A wave by wave analysis of some simulated wave data (uni-directional) was carried out to look at the distribution of the wave excursion amplitudes. The calculations were based on the simulated wave data for a uni-directional spectrum because of the difficulties which arise in defining the wave period for a directional spectrum (where the period of one component is not necessarily the same as another component). The wave excursion amplitude, A_{wave}, was calculated for each wave according to

$$A_{wave} = \frac{U_{m,wave}\, T_{wave}}{2\pi} \qquad (7)$$

where

$U_{m,wave}$ = maximum bottom orbital velocity for the individual wave
T_{wave} = wave period for the individual wave

A Rayleigh distribution was fitted to the calculated distribution for A, with

$$A_R = \frac{\sqrt{2}\,U_{rms}T_p}{2\pi} \qquad (8)$$

By definition, the value of A at the peak of the Rayleigh distribution is

$$A_{peak} = \frac{A_R}{\sqrt{2}} = \frac{U_{rms}T_p}{2\pi} \qquad (9)$$

Figure 6 shows two examples of the distribution of A from a wave by wave analysis of simulated wave data, with the corresponding Rayleigh distributions. As the Rayleigh distributions were a satisfactory fit to the calculated distributions, the Rayleigh distribution was used to calculate a probability-weighted value of the friction factor, f_w, for a wave spectrum. It was found that using the Soulsby power law (Equation 5) the ratio of the weighted fraction factor, f(weighted), to the friction factor calculated using A_{peak} , $f(A_{peak})$, was constant at 1.04. Using the Swart law (Equation 4) the ratio varied from 0.95 to 1.4, depending on the value of A/z_0.

As mentioned earlier, these calculations were based on simulated wave data. However, the results are in terms of parameters which are standard for a multi-directional spectrum so can be applied generally. It was therefore decided to use the Soulsby formula for calculating the wave friction factor and that the value calculated by using A_{peak} was satisfactory for the complete spectrum of waves.

3.2 Waves plus current

3.2.1 Existing theories

To calculate the bed shear stress under combined waves and currents there are two distinct approaches. The first, as adopted by Grant and Madsen (1979), and Bailard (1981), is to assume that the shear stress for the combined wave and current can be expressed as a quadratic function of the combined wave and current velocity at some height above the bed. Thus

$$\underset{\sim}{\tau}(t) = \rho f_{w+c} |\underset{\sim}{U}(t)| \, \underset{\sim}{U}(t) \tag{10}$$

where

f_{w+c} is a friction coefficient for the combined wave plus current applicable at the height at which U is measured. However, f_{w+c} is not equal to the drag coefficient, C_D, which is usually calculated for the mean current velocity nor to half the wave friction factor, $f_w/2$, which is calculated for a wave velocity within the wave boundary layer. The difficulty lies in finding a height at which a single value of the friction coefficient applies.

The second approach, as adopted by Christoffersen and Jonsson (1985), is to treat the wave and current contributions to the shear stress entirely separately, expressing each part as a quadratic function of the velocity (current or wave).

Thus

$$\begin{aligned} \underset{\sim}{\tau}(t) &= \underset{\sim}{\tau}_{c+} + \underset{\sim}{\tau}_{w+}(t) \\ &= \rho C_{D+} |\bar{\underset{\sim}{U}}| \, \bar{\underset{\sim}{U}} + \frac{1}{2} \rho f_{w+} |\underset{\sim}{u}(t)| \, \underset{\sim}{u}(t) \end{aligned} \tag{11}$$

where

$\bar{\underset{\sim}{U}}$ = time-mean current velocity at the height applicable to the drag coefficient

C_{D+} = drag coefficient, possibly enhanced by waves

$\underset{\sim}{u}(t)$ = wave velocity

f_w+ = wave friction factor, possibly enhanced by current

Under the EC funded Marine Science and Technology programme (MAST), G6M Coastal Morphodynamics, a comparison of numerical models for shear stress under combined waves and currents was made between the participating institutes (Soulsby et al, 1993). The models dealt only with regular waves but all models showed both enhancement of the current induced shear-stress by the waves, and enhancement of the wave induced shear stress by the current. As part of the study the mean shear stress, τ_m, and the maximum shear stress, τ_{max}, from each of the models were parameterised in terms of the relative wave and current strengths, using the same general formulae.

The relative strengths of the wave and current were expressed as a parameter x where

$$x = \frac{\tau_c}{\tau_c + \tau_w} \tag{12}$$

where τ_c is the shear stress calculated for a current alone and τ_w is the shear stress calculated for the wave alone (see Figure 7). The mean and maximum shear stresses were then expressed as

$$y = \frac{\tau_m}{\tau_c + \tau_w} = x(1 + bx^p(1-x)^q) \tag{13}$$

and

$$Y = \frac{\tau_{max}}{\tau_c + \tau_w} = 1 + ax^m(1-x)^n \tag{14}$$

where

a, m, n, b, p, and q are coefficients which were optimised for each model.

Coefficient a was given by:

$$a = (a_1 + a_2|\cos\phi|^I) + (a_3 + a_4|\cos\phi|^I)\log_{10}(f_w/C_D) \tag{15}$$

with analogous expressions for m and n.

Coefficient b was given by:

$$b = (b_1 + b_2|\cos\phi|^J) + (b_3 + b_4|\cos\phi|^J)\log_{10}(f_w/C_D) \tag{16}$$

with analogous expressions for p and q. The constants a_1 to a_4 etc and powers I and J were optimised to give the best overall fit to the model results for all ϕ, the angle of the waves relative to the current.

The parameterisation of these models can be used to look at either of the two approaches outlined above.

3.2.2 *Calculation of 'combined' friction factor from parameterised numerical models*

The Grant and Madsen approach was tested for the field data from Isle of Wight and Norfolk Sand Banks. Using the Isle of Wight data, in which velocities were recorded 0.10m above the bed, a friction coefficient was defined in a similar manner to Equation 10:

$$\underset{\sim}{\tau}(t) = \rho f_{10} \underset{\sim}{U}(t) \, |\underset{\sim}{U}(t)| \tag{17}$$

where $\underset{\sim}{U}(t)$ is the combined wave and current velocity vector.

A maximum shear stress can be written as

$$\tau_{max} = \rho f_{10} U_{max}^{2} \tag{18}$$

where

$$U_{max}^{2} = (U_{10} + W\cos\phi)^2 + W^2\sin^2\phi \tag{19}$$

U_{10} is the mean current speed at 0.10m
W is the maximum orbital velocity of a regular wave at 0.10m
ϕ is the angle of the waves relative to the current

U_{max} is the resultant from the vector addition of the current velocity and the maximum wave velocity.

For each burst of the Isle of Wight data, U_{10}, U_{rms} and ϕ are known. Writing

$$W = \sqrt{2}\, U_{rms} \tag{20}$$

defines a regular wave of maximum orbital velocity W with the same root-mean-square orbital velocity as the irregular wave defined by U_{rms}. U_{max} can then be calculated according to Equation 19. U_{10} and W can also be used to calculate the current only shear stress τ_c and the wave only shear stress τ_w respectively (Figure 7), using an appropriate value of z_0 for the site (0.001m for IOW data). These can be used in Equations 12 and 14 to calculate the maximum shear stress according to the parameterised models. In this study the coefficients used were those calculated in the MAST study (Soulsby, 1993) for the model of Davies, Soulsby and King (1988).

Then using τ_{max} from Equation 14 and U_{max} from Equation 19, the friction coefficient f_{10} can be calculated from Equation 18.

Using a range of values for U_{10}, W (= $\sqrt{2}\, U_{rms}$), T_p and ϕ typical of the Isle of Wight deployment, a range of different values of f_{10} were calculated using the above method. These were plotted against the relative strengths of the wave and current using the index x (Equation 12).

This method was also used for the Norfolk Sand Banks data, except that all measurements were made at 0.41m and a different z_0 was used (0.0004m). The results of friction coefficient for both sites are shown in Figure 8. If the

Grant and Madsen approach (as given by Equation 17) is to be valid for any instantaneous velocity at the selected height, then the friction coefficient (f_{10} or f_{41}) should be constant. Both sets of results show considerable scatter as the flow becomes more wave dominated. In each case, at the current dominated end, f_{10} would eventually tend to the value of the drag coefficient calculated for a current alone. Furthermore, the results showed no obvious way to parameterise f_{10} in terms of U, U_{rms}, T_p and ϕ. Using the mean value of f_{10} at any value x could result in errors of 50-100% for wave dominated flows. This would also result in 50-10% error in the shear stress, with large errors introduced into the calculation of sediment transport.

As the variation in the predicted friction factor was so large it was decided to adopt the second approach (Christoffersen and Jonsson) of separating the wave and current contributions to the shear stress. However, it should be noted that experimental evidence favouring the "Grant and Madsen" approach was provided recently by Arnskov et al (1993), whose measured bed shear-stress locus for perpendicular waves and currents over a smooth bed showed a parabolic form, similar to Equation 10, rather than the rectilinear form of Equation 11.

3.2.3 Enhancement of wave shear stress due to current

At present, there are few experimental studies which have measured shear stresses directly and which have therefore been able to contribute to the discussion on whether the current enhances the wave contribution to the shear stress. However, recent studies in a large wave basin at HR Wallingford, carried out by University College London (UCL), investigated the effect of a current flowing at right angles to the waves. Both regular waves (Simons et al, 1992) and irregular waves (Simons, Pers. Comm.) were investigated. Measurements of three components of velocity were made at several heights above the bed as well as direct measurements of shear stress using a shear plate mounted on the bed. Although the waves generated in each test were a random sequence, the same random generator seed was using to start the wave sequence so that the same random sequence could be repeated for waves only and for waves plus current. Figure 9 shows an example of velocities recorded in the current (u) and wave (v) directions for a short sequence of waves, without and then with a current of approximately $0.1 ms^{-1}$. Figure 10 shows two examples of the shear stress measured directly in the wave only and wave plus current cases. A correction has been made to the shear stress by UCL to remove the pressure effect on the shear plate. In both the examples shown the current appears to increase the peaks of shear stress by a small amount, although for regular waves Simons et al. (1992) suggest no enhancement of the shear stress. However, the current is perpendicular to the waves so enhancement may be expected to be small.

All the numerical models used in the MAST inter-comparison exercise indicated enhancement of the wave shear stress by the current. In the present study, the parameterised models were used to compare the maximum shear stress calculated by the models to the maximum shear stress which would be achieved if the wave shear stress were not enhanced.

τ_{max} 'full' (ie from parameterised model) was defined as in Equation 14. A τ_{max} 'simple' was defined by assuming that the wave shear stress, τ_w, was unenhanced by the addition of a current, and that the angle ϕ of wave shear stress was also affected. Then:

$$\tau_{max,simple} = [(\tau_m + \tau_w\cos\phi)^2 + (\tau_w\sin\phi)^2]^{0.5} \tag{21}$$

This is equal to the magnitude of the vector resulting from the vector addition of τ_m and τ_w (as shown in Figure 7).

Y_{simple} was then defined as:

$$Y_{simple} = \frac{\tau_{max,simple}}{\tau_c + \tau_w} \tag{22}$$

The ratio Y_{simple}/Y_{full} was calculated for a range of values of x, ϕ, f_w and C_D and for several of the parameterised models.

Figure 11 shows the effect of increasing A/z_0 (which decreases f_w) or increasing z_0/h (which increases C_D) for the model of Fredsøe (1984). Both of these changes have only a very small effect on the ratio Y_{simple}/Y_{full} and a much larger effect is seen with the variation in x and ϕ. The ratio is lowest for the case of co-linear waves and currents (ϕ=0°) and for a value of x around 0.7 (ie more towards the current dominated end), when the 'simple' formulation for maximum shear stress underestimates the 'full' maximum shear stress by around 35%.

Using the parameterisation for several different models given in Soulsby et al (1993) the ratio was calculated for the models of Fredsoe (1984), Huynh-Thanh and Temperville (1991) and Myrhaug and Slaattelid (1990), and shown in Figure 12. In all cases the ratio is less than one, particularly when both waves and current are approximately equal strength and in the same direction. In the worst case, the 'simple' formulation underestimates by between 20% and 35%.

On the basis of both the UCL data and the above model results, it was decided that some enhancement of f_w by a superimposed current probably does occur, and the use of an unenhanced f_w in Equation 11 would give unacceptably large errors in $\tau(t)$. The following method of predicting $\tau(t)$, in which both C_{D+} and f_{w+} are enhanced in a manner which gives agreement with the full boundary layer models for τ_m and τ_{max}, was therefore adopted.

At present, the parameterised models are the best indication of how much the wave shear stress is enhanced under a range of different conditions. The instantaneous shear stress vector was calculated from the mean and fluctuating velocity using Equation 11, where the enhanced drag coefficient, C_{D+}, and wave friction factor, f_{w+}, were deduced from the models using:

$$C_{D+} = \frac{\tau_m}{\rho\bar{U}^2} \tag{23}$$

where

τ_m is calculated from the model
$\bar{U}$ is the mean current speed

and

$$f_{w+} = \frac{\tau_{w+}}{0.5\rho W^2} \tag{24}$$

where

τ_{w+} is in the direction of the wave velocity and is calculated from a vector subtraction

$$\underset{\sim}{\tau}_{w+} = \underset{\sim}{\tau}_{max} - \underset{\sim}{\tau}_m \tag{25}$$

where

τ_{max} is calculated from the model
W is the maximum orbital velocity of an equivalent regular wave (= $\sqrt{2}\ U_{rms}$).

The time series of shear stress is then calculated from

$$\underset{\sim}{\tau}(t) = \underset{\sim}{\tau}_m + \underset{\sim}{\tau}_{w+}(t) \tag{26}$$

with

$$\begin{aligned} \underset{\sim}{\tau}_m &= \rho C_{D+} |\underset{\sim}{\bar{U}}|\, \underset{\sim}{\bar{U}} \\ \underset{\sim}{\tau}_{w+} &= \frac{1}{2} \rho f_{w+} |\underset{\sim}{u}(t)|\, \underset{\sim}{u}(t) \end{aligned} \tag{27}$$

$\underset{\sim}{u}(t)$ is the orbital velocity time series.

A step-by-step procedure for the method is given in Appendix 1.

The time series for the corresponding regular wave was also calculated according to Equations 26 and 27. In this case the time series of orbital velocity is calculated from:

$$\underset{\sim}{u}(t) = \sqrt{2} U_{rms} \sin\left(\frac{2\pi t}{T_p}\right) \begin{pmatrix} \cos\phi \\ \sin\phi \end{pmatrix}$$

3.2.4 Comparison of combined shear stress distribution for irregular and regular waves

The method described above was used to calculate time series of shear stress for both irregular waves and a corresponding regular wave using the field data collected from the Isle of Wight.

A comparison of the probability distribution of resulting shear stresses is shown for two examples in Figure 13. For the most frequently occurring shear stresses the distributions match reasonably well, but the shape of the distributions is quite different. It is apparent that the irregular wave bed shear stresses have occasional contributions far in excess of the maximum values under the regular wave. These have consequences for the net sediment transport, and it can be seen that it is not strictly possible to choose any regular wave which will exactly correspond to the behaviour of the irregular waves. In particular, if the critical shear stress for motion of the sediment just exceeds the maximum shear stress generated by the regular wave (eg if τ_{cr} = 3.0Nm^{-2} for burst 34, lower part of Figure 13) then the regular wave will allow no sediment transport. In contrast, for the irregular waves, the shear stress exceeds 3.0Nm^{-2} for a significant proportion of the time (approximately 11% of the time for burst 34, lower part of Figure 13), and hence would give rise to significant sediment transport.

Figure 14 shows a scatter plot of shear stresses for burst 13 (Norfolk Sand Banks), a burst during which the current was small. The shear stresses from the irregular waves can be seen to exceed those of the corresponding regular wave for a considerable proportion of the time. Figure 14 also shows the critical shear stress required to move sediment of grain sizes 200µm, 500µm, 1mm and 2mm. For shear stresses lower than the critical value, no sediment is moved. In this case, for a grain size of 2mm, the regular wave would allow no transport at all, whereas the irregular waves quite frequently fall outside this "exclusion zone". The largest waves generate shear stresses approximately three times the critical value. It can be seen that, in this particular case, the corresponding regular wave would not give a good approximation to the sediment transport.

3.2.5 Comparison of combined shear stress for observed data and calculated data

Figure 15 shows the time series of shear stress calculated according to Appendix 1 using the velocity data provided from the UCL laboratory tests. The figure also shows the observed shear stress recorded by the shear plate (the correction for pressure on the plate has been applied, but not for the direct pressure force on the grains attached to the plate). The method in Appendix 1 will always result in shear stresses in phase with the velocity. However, the observed shear stress leads the velocity by a significant phase shift (Simons, 1993) which has been removed for the purpose of this comparison. For the purposes of calculating mean sediment transport over periods of 10-60 minutes this phase shift is unimportant.

For the very short sequence of waves shown here, the calculated shear stress appears to match the observed shear stress quite well at the large peaks, but underestimates significantly at smaller peaks. Deficiencies in the degree of correspondence may possibly be associated with the pressure force on the grains on the shear plate.

4 Calculation of bed load sediment transport

4.1 Method

Bed load transport was calculated for both the irregular waves and the corresponding regular waves using the time series of shear stress. The instantaneous dimensionless bed load transport vector $\underset{\sim}{\Phi}_b(t)$ was calculated from a formula given by Soulsby (1993), with an assumption that $\underset{\sim}{\Phi}_b(t)$ is in the same direction as $\underset{\sim}{\tau}(t)$:

$$\underset{\sim}{\Phi}_b(t) = 12|\underset{\sim}{\theta}(t)|^{\frac{1}{2}}(|\underset{\sim}{\theta}(t)| - \theta_{cr})\frac{\underset{\sim}{\theta}(t)}{|\underset{\sim}{\theta}(t)|}H(|\underset{\sim}{\theta}(t)| - \theta_{cr}) \tag{29}$$

where

$$\underset{\sim}{\Phi}_b = \frac{\underset{\sim}{q}_b}{\sqrt{g(s-1)d^3}} \tag{30}$$

$\underset{\sim}{q}_b(t)$ = volumetric bedload sediment transport rate (m^2s^{-1})
$\underset{\sim}{\theta}(t)$ = the dimensionless bed shear stress (Shields parameter) given by

$$\underset{\sim}{\theta}(t) = \frac{\underset{\sim}{\tau}(t)}{g\rho(s-1)d} \tag{31}$$

g = acceleration due to gravity (9.81 ms^{-2})
ρ = water density (1000 kg m^{-3})
s = specific grain density (2.65)
v = viscosity (1.36 10^{-6} m^2s^{-1})
d = grain diameter (m)
θ_{cr} = dimensionless shear stress for threshold of motion

The transport is "switched off" when the shear stress falls below the threshold of motion by means of the Heaviside function, H(x), defined as:

$$\begin{aligned} H(x) &= 0, \quad \text{for } x \le 0 \\ H(x) &= 1, \quad \text{for } x > 0 \end{aligned} \tag{32}$$

θ_{cr} was calculated according to Soulsby (1993) using the formula

$$\theta_{cr} = \frac{0.0666D_* + 0.375}{2.22D_* + 0.938} \tag{33}$$

where D_* is the dimensionless grain diameter, given by

$$D_* = \left[\frac{g(s-1)}{v^2}\right]^{\frac{1}{3}} d \tag{34}$$

The mean volumetric sediment transport vector was then calculated as:

$$\overline{\underset{\sim}{q}}_b = \sqrt{g(s-1)d^3}\ \frac{1}{T}\int_0^T \underset{\sim}{\Phi}_b(t)dt \tag{35}$$

Sediment transport under both irregular waves and regular waves was calculated in this way. For irregular waves, T is the duration of the whole record; for regular waves, T is the wave period.

The ratio of the vector magnitudes was then calculated:

$$r_q = \frac{|(q_b)_{irreg}|}{|(q_b)_{reg}|} \tag{36}$$

The effect of bedforms (eg ripples) is neglected throughout. Thus we assume that either sheet flow conditions apply, or that the skin friction component of bed shear stress is used in Equation 31, and that this is given (at least approximately) by the procedure in Appendix 1.

4.2 Sensitivity tests using simulated wave data

Simulated wave data was used in sensitivity tests to investigate the effect of changing various parameters on the mean sediment transport. This enabled the parameters to be changed in a controlled manner and also to extend the range of variables beyond the ranges shown in the observed data from Isle of Wight and Norfolk Sand Banks.

The computer program which generated the "synthetic" wave data was written by Martin Mathiesen of SINTEF NHL (Norwegian Hydrotechnical Laboratory). Given a set of parameters to define a random wave spectrum it calculates a time series of surface elevation and orbital velocities at any chosen height in the water column. A random number generator is used to give each wave a random phase. A different random seed can be used to start the random generator process, thus generating sample sequences from a population with the same statistical properties. Thus the actual significant wave height and peak period will not necessarily be exactly the same as the input variables, particularly for a short sequence. This allowed investigation of the statistical variation of a sample sequence from a population with the same statistical properties, which is an important factor when assessing whether observed data is representative of the conditions over a longer period of time.

The model was slightly modified to allow input of a mean current velocity, which was used when calculating shear stresses and sediment transport.

A standard set of input conditions was chosen as the base for comparison. The standard input variables were:

Water depth	10.0m
Significant wave height	5.0m
Peak period	10s
Spectrum	JONSWAP
γ, defining spectrum shape	3.3
Mean wave direction	45°
Directional spread	30°
Number of data points	4096
Time interval	0.5s
Number of frequencies	1000
Number of directions	40
Random generator seed	1
Mean current, $\bar{\underset{\sim}{U}}$	(1.0,0.0) ms^{-1}
Height of velocity time series	1.0m above bed

Sensitivity tests were run to investigate the effect of changing the random generator seed, the mean current, the wave height, the wave period, the mean wave direction, the spectrum shape and the directional spread. In all these cases the grain diameter was taken to be 200µm.

Figure 16 shows the effect of changing the random generator seed on the magnitude of mean transport by irregular waves, q_{irreg} (upper figure) and on the ratio r_q (lower figure). The runs are labelled 0 - 29 for identification between the two plots. The statistical variation in the significant wave height is shown by the variation in the root-mean-square orbital velocity, U_{rms}, which results in a trend of increasing sediment transport with increasing orbital velocity. However, the true statistical variation is shown by the deviation from this trend, so that the ratio is approximately the same for runs 2 and 8 (the extremes of U_{rms}). The ratio r_q varies between approximately 0.95 and 1.01 for this set of standard conditions. The ratio of the mean transport (irregular) summed over all runs to the mean transport (regular) was 0.981. This represents the value of the ratio which would be calculated if all the time series had been combined together into one long record (approximately 17 hours long). The standard deviation was 0.0139, which indicates the effect of taking a much shorter record as a "representative" sample.

The effect of changing the mean current between $0.5ms^{-1}$ and $1.5ms^{-1}$ is shown in Figure 17. The increase in current changes both the magnitude of the mean sediment transport and the ratio r_q in a systematic way. The sediment transport rate increases by about an order of magnitude over this range whereas the ratio increases from approximately 0.97 to 1.01, which is within the range indicated by the statistical variation.

Figure 18 shows the effect of increasing the significant wave height from 1.0m to 6.0m. The increase in the mean sediment transport rate is approximately a factor of three, and the ratio decreases from 1.02 to 0.99. Again, this is the same order of variation as the statistical scatter. The wave period was also changed in a separate set of tests within the range 8s to 12s. The effect of changing the period means that the random phases are given to different waves, so the statistical variation of the random generator seed also affects these results. However, the variation was small (r_q from 0.96 - 0.99).

The direction of waves relative to the current is varied in Figure 19. Once again the ratio only varies within the range 0.95 - 1.02 (upper figure). The lower figure shows the variation in the direction of the mean sediment transport, which shows a variation from approximately 0° for $\phi = 0°$ and $\phi = 90°$ to around 5° for $\phi = 45°$. In all cases the direction of mean transport was swung from the mean current direction <u>towards</u> the angle ϕ, but the swing was smaller for irregular than regular waves.

The effect of changing the spectrum shape was considered by changing γ from 3.3 (for a JONSWAP spectrum) to 1.0 (for a Pierson Moskowitz spectrum). This had less than 1% effect on the ratio r_q or on the magnitude of the sediment transport. The directional spreading was also changed from 30° to unidirectional waves. This did not affect the magnitude or ratio at all and the only identifiable difference was a small change (< 1°) in the direction of the mean sediment transport (irregular).

The results of the sensitivity tests indicate that, for these standard tests, the ratio r_q is approximately 1.0 ± 6%, which is well within the usual acceptable range for sediment transport calculations.

4.3 Effect of grain size

The sediment transport rates for grain sizes of d=200µm, 2mm and 2cm were calculated using the 30 shear stress time series generated using the computer program with different random seeds. This showed the statistical variation of the results for each of the different grain sizes. The critical shear stress for movement of the sediment was $0.22Nm^{-2}$ (d=200µm), $1.13Nm^{-2}$ (d=2mm) and $10.13Nm^{-2}$ (d=2cm). In each case, the value of z_0 used in the calculation of the drag coefficient C_D and the friction factor f_w (and hence in the calculation of shear stress) was taken to be:

$$z_0 = \frac{d}{12} \qquad (37)$$

where

d = grain size

The increase in grain size resulted in a corresponding increase in the mean shear stress (varying from an average of $2.4Nm^{-2}$ for d=200µm to $7.3Nm^{-2}$ for d=2cm). The maximum shear stress predicted by the parameterised model (for a regular wave) was also considerably increased (from around $6.5Nm^{-2}$ for d=200µm to $44Nm^{-2}$ for d=2cm).

Figure 20 shows the magnitude of the mean sediment transport rate under irregular waves for the 30 different samples, for each grain size (upper figure) and the ratio of the irregular transport rate to the regular transport rate (lower figure). It is noteworthy, but surprising, that the magnitude of the transport rate increased with grain size, in spite of the fact that the threshold of motion also increased. This occurs because the shear stresses increase with increasing grain size more rapidly than the threshold shear stress does in Equation 29. This behaviour would occur for any bedload transport relation of the general form $\Phi_b \sim \theta^{3/2}$. The physical validity of this result is open to question; however, for the present purpose of examining the ratio of q_{irreg} to q_{reg}, this effect largely cancels out. It can be seen that it is mainly the waves which are causing the increased transport rates, since if there were no waves at all, the current alone would not generate a large enough shear stress to move the 2cm sediment at all (especially as the value of the mean shear stress, τ_m, given above already includes some enhancement due to waves). As the grain size increased there was more scatter in the magnitude of the sediment transport rate. This can be attributed to the fact that as the critical shear stress increased more of the smaller waves can no longer contribute to the transport, so that the irregularity of the larger waves is more dominant.

The ratio of irregular to regular transport rates showed a trend of decreasing with an increase in grain size. The mean ratio decreased from 0.98 (d=200µm) to 0.94 (d=2mm) to 0.84 (d=2cm). The increase in scatter as the grain size decreased was also apparent in the ratio. Because there was quite a large current in these test cases ($1.0ms^{-1}$) this means that the shear stresses for the regular wave were entirely outside the "exclusion zone" resulting from the threshold of motion (at least for the smaller grain sizes). However, because of the directional spreading of the irregular waves, an increasing proportion of them fell within the exclusion zone and therefore no longer contributed to the transport. It could be expected that as more of the shear stresses from the regular wave fall within the "exclusion zone" the ratio would increase, and in the case where virtually all of the regular wave fell within the "exclusion zone" the ratio could be very much greater than 1.

For the range of shear stresses and grain sizes used in these test cases, the ratio of irregular to regular transport rates was still mainly within the range 1.0 ± 20%, and therefore the method of calculating sediment transport described above is still recommended for this range of grain sizes.

4.4 Field data

Sediment transport rates were calculated from the STABLE velocity data for the Isle of Wight and Norfolk Sand Banks. In each case the shear stress time series were calculated using a value of z_0 calculated previously from the velocity data. The resulting time series should represent the shear stresses which were actually present at each site. However, the grain size used for both sites in the calculation of sediment transport was 0.0002m, which may be suitable for the sediment at Norfolk Sand Banks. The bed at the Isle of Wight was immobile gravelly sand, so the sediment transport rates calculated here only represent what could theoretically be transported.

Parameters used in calculating the shear stresses were:

	Isle of Wight	Norfolk Sand Banks
Water depth	25m	29m
z_0	0.001m	0.0004m
Height of velocity measurements	0.10m	0.41m

The STABLE data was logged at 4Hz. Data for each component of velocity was stored as a mean value and a time series of fluctuations about the mean. For these calculations, the velocity time series were filtered to remove the high frequency turbulence using a half-power point of 1Hz. The filtered fluctuations still included low frequency turbulence which could be attributed to the current. However, this was left in as it was felt that this would have an effect on the sediment transport anyway. The root-mean-square of the fluctuations, denoted U_{rms}, included this low frequency turbulence.

The mean sediment transport rates for irregular (observed) waves and the corresponding regular waves were compared for each burst and each site. The procedure was the same as for the synthetic data. Pairs of figures are presented to show the results from the Isle of Wight and Norfolk Sand Banks together.

Figure 21 shows the observed shear stress (from Tables 1 and 2) against the mean shear stress calculated from the time series for the irregular wave. The Isle of Wight data shows a very good one-one linear relationship, which indicates that the method for calculating shear stress used in this study gives results of the right magnitude. The Norfolk Sand Banks data shows smaller predicted stresses than observed, possibly because the value of z_0 was underestimated (no current-alone data was available for NSB). However, this should not affect conclusions about the ration r_q.

The magnitude of the sediment transport rate appears to be heavily dominated by the mean current (Figure 22). The data for the individual bursts are shown as symbols; the solid curve shows the sediment transport which would be calculated for a current alone (using the unenhanced drag coefficient C_D). For both the Isle of Wight and Norfolk Sand Banks, the current-only curve shows a threshold for the current below which there is no transport. A different threshold for the current is shown at the two sites because of the different value of z_0 which is used in the calculation of C_D, and because the currents for the two sites are measured at different heights. However, the calculated data points show that the presence of the waves combined with the low current does allow some transport. Just above the threshold, the waves enhance the transport by a factor of 2 - 3. At higher currents, the enhancement of sediment transport by the waves is less pronounced, but still increases the transport by a factor of up to 1.5 for the Isle of Wight. The enhancement is up to a factor of 2 for Norfolk Sand Banks, where the waves are larger than at IoW.

The increase in the magnitude of the sediment transport is less obvious when plotted against U_{rms} (Figure 23). As mentioned above, U_{rms} includes the low frequency fluctuations in velocity which could be attributed to the current, so there is a trend of increasing U_{rms} with increasing current, which is reflected in the increase of sediment transport rate with increasing U_{rms}. However, there is much more scatter than for the current, with the unusual bursts giving atypical results. These bursts have been identified in Figure 23 by their burst number, so that unusual features of the burst can be found in Tables 1 (IOW) and 2 (NSB). Tables 1 and 2 give summaries of each burst in terms of the data used in these calculations: mean current, U_{rms}, direction of waves relative to current. The value of σ_{wave} shown in the table is the root-mean-square of the fluctuations due to the waves only. It was calculated in the original studies by a technique of spectrum splitting (Soulsby and Humphery, 1989). It is included for comparison with the U_{rms} values used in this study, which include some turbulence due to the current as well as the waves. The table also includes the mean bed shear stress which was calculated from the original data which can be compared with the mean bed shear stress calculated from the time series of shear stress in this study.

Figure 24 shows the ratio r_q against the mean current for both the Isle of Wight and Norfolk Sand Banks. In both cases, provided the current is not small (> approximately 0.2ms^{-1}), the ratio of irregular to regular transport is approximately 1.0 ± 0.2. The deviation from this ratio occurs when the flow is wave dominated, when the ratio is either much higher or much lower than 1, with no consistent features between bursts on either side of the ratio 1.0. Most of the bursts with very low currents still have significant wave activity so the deviation from the ratio 1.0 may be due to the asymmetry of the irregular wave in comparison to the regular wave. This will appear more obvious when there is little current because the effect of the critical shear stress for threshold of motion will mean that only the larger waves can contribute to the sediment transport.

Figure 25 shows the difference in direction between the mean transport under irregular waves and the transport under regular waves. Apart from the heavily wave dominated flows, the difference in direction is only approximately ±10°. Larger deviations occur for the wave dominated bursts, when the direction of the mean transport under irregular waves can be affected by a few large waves.

Figure 26 summarises the comparison of the magnitude of the sediment transport rate computed for the equivalent regular wave with that for the irregular waves for the Isle of Wight and Norfolk Sand Banks data sets. the data shows relatively little scatter about the line of perfect agreement, with the percentage errors being smaller for larger transport rates, indicating that the specification of the equivalent regular wave must be close to optimum.

5 Conclusions and recommendations

5.1 Conclusions

1. A linearised formulation for shear stress (Equation 2) is inadequate for sediment transport, with the "true" quadratic shear stress exceeding the linearised stress for approximately 32% of the time. 5% of the time the quadratic stress exceeds the linearised stress by a factor of 2 to 3.

2. The wave excursion amplitudes for an irregular wave spectrum form a Rayleigh distribution, with a peak at $A_{peak} = U_{rms}T_p/2\pi$. Calculation of a wave friction factor using A_{peak} gives a satisfactory approximation to a weighted friction factor calculated from the probability distribution (to within 4% when using the power law, Equation 5).

3. If the shear stress $\tau(t)$ is written as a quadratic function of the total velocity (wave plus current) at some height. ie

   $$\underset{\sim}{\tau}(t) = \rho f_{w+c} |\underset{\sim}{U}_{w+c}(t)| \underset{\sim}{U}_{w+c}(t) \qquad (38)$$

   then a friction coefficient can be calculated using the parameterised models from MAST G6M. For a range of values of mean current, wave orbital velocity, wave direction and wave period, the resulting friction coefficient varies by more than a factor 3. Even if the friction coefficient were made to be a function of the relative wave-current strength (x), it would vary by 50-100% for wave dominated flows and by around 20% for current dominated flows. This is considered too large a variation for calculation of shear stress by this method to be acceptable.

4. Laboratory measurements (by University College London) of shear stress under waves only and waves plus current (current at right angles to the waves) indicate a small enhancement of the peak shear stresses when the current is added. The wave plus current boundary layer models parameterised in MAST G6M all indicate enhancement of the shear stress fluctuations when a current is added. The amount of enhancement is not significantly changed by variation in A/z_0 or z_0/h but varies between models. The worst case is when the waves and currents are approximately equal strength, when the maximum shear stress is underestimated by between 20% and 35% if an unenhanced wave shear stress is assumed.

5. A time series of shear stress for a current $\underset{\sim}{\bar{U}}$ plus an irregular wave velocity $\underset{\sim}{u}(t)$ can be calculated from

$$\underset{\sim}{\tau}_{irreg}(t) = \rho C_{D+} |\underset{\sim}{\bar{U}}| \underset{\sim}{\bar{U}} + \frac{1}{2}\rho f_{w+} |\underset{\sim}{u}(t)| \underset{\sim}{u}(t) \tag{39}$$

where C_{D+} and f_{w+} are deduced from the MAST G6M parameterised models. A step-by-step procedure is given in Appendix 1.

A time series of shear stress for an equivalent regular wave, $\tau_{reg}(t)$ can be also be calculated from Equation 39, using

$$\underset{\sim}{u}(t) = \sqrt{2}\, U_{rms} \sin\left(\frac{2\pi t}{T_p}\right)\begin{pmatrix}\cos\phi \\ \sin\phi\end{pmatrix} \tag{40}$$

in place of the irregular wave velocity time series.

The frequency distributions for irregular and regular waves match well (Figure 13) for the commonest waves, but the irregular shear stresses occasionally exceed the maximum regular stress by a factor of 2.

6. Synthetic wave data was used for sensitivity tests to investigate the effect of changing the random generator seed, the mean current, the wave height, the wave period, the mean wave direction, the spectrum shape and the directional spread. For a set of standard conditions changing the random generator seed (which changes the random phase given to each wave) changed the ratio r_q (mean irregular transport / mean regular transport) between 0.95 and 1.01 (Figure 16). This indicates the statistical variation which may be expected when taking a short record (34 minutes in this case). 30 samples with different random seeds gave a mean ratio of 0.981 and a standard deviation of 0.0139. This represents the value of the ratio which would result from a long record (17 hours in this case). An 8.5 minute record would be expected to have twice as great a statistical scatter (ie 95% confidence limits of up to ± 6%).

Changing the mean current (Figure 17), the wave height (Figure 18), the wave direction (Figure 19), the spectrum shape and directional spread all resulted in changes to the ratio r_q which were less than or similar to the statistical variation due to the random seed. A ratio of 1.0 ± 0.06 was adequate to cover all these variations in parameters.

7. An increase in the grain size resulted in an increase in the magnitude of the shear stresses. Although the critical shear stress for motion of the sediment also increased, the magnitude of the bedload sediment transport rate increased with grain size. The ratio irregular to regular transport (r_q) decreased with grain size (from an average of 0.98 for d=200µm to 0.84 for d=2cm). This was attributed to the more dominant effect of the larger irregular waves as more of the smaller waves fall inside the "exclusion zone" defined by the critical shear stress (and therefore no longer contribute to the transport).

8. Velocity data collected from STABLE deployments at Isle of Wight and Norfolk Sand Banks were used to investigate the ratio r_q. Provided the current was greater than approximately $0.2ms^{-1}$, the ratio r_q was in the range 1.0 ± 0.2. For low currents and wave dominated flows the ratio was much higher or much lower than 1 with no consistent features to classify bursts lying either side. Apart from the wave dominated bursts, the difference in direction between the mean transport under irregular waves and the mean transport under regular waves was ± 10°.

   The magnitude of the sediment transport rate is heavily dominated by the size of the mean current. The presence of the waves causes an enhancement of the transport rate by a factor of 2 to 3 near the threshold of motion and by 1.5 to 2 for larger currents. The waves allow some sediment transport even below the threshold of motion for current only.

5.2 Recommendations

The net bedload transport rate of sediment under currents plus irregular waves can be approximated by the use of suitably defined equivalent regular waves to better than ± 20% in magnitude and ± 10° in direction. The regular wave should have an orbital velocity amplitude of $\sqrt{2}U_{rms}$, a period of T_p, and a direction equal to the mean direction of the full irregular wave spectrum.

The replacement of the irregular waves by an equivalent regular wave reduces the numerical integration of the time-series from several thousand data points to about 20 (i.e. one wave cycle). However, considerably greater computational savings, as well as greater physical insight, would be gained by approximating the numerical integration of the bedload transport formula by an algebraic function. This approach is being pursued by the second author in a separate study.

The results of this work would be strengthened by using a full boundary layer model to investigate the accuracy of the method for calculating shear stress under irregular waves. The model would also be able to predict suspended sediment transport, in addition to bedload transport, under irregular and regular waves, which would add additional information to this study. This work is currently being undertaken by Dr A G Davies of Bangor University, in coordination with the present study.

6 Acknowledgements

The authors gratefully acknowledge:

Proudman Oceanographic Laboratory, Bidston - for allowing use of the data collected in the Norfolk Sand Banks study

Mr Martin Mathiesen of SINTEF NHL (Norwegian Hydrotechnical Laboratory, Trondheim) - for providing the program for simulated wave data

Dr R R Simons (University College London) - for providing laboratory data on shear stresses measured under waves and currents

Mr R Austin (Institute of Hydrology, Wallingford) - for providing simulated data for a unidirectional and multidirectional spectrum

7 References

Arnskov, M. M., Fredsøe, J., and Sumer, B. M., 1993. Bed shear stress measurements over a smooth bed in three-dimensional wave-current motion. Coastal Engineering, 20: 277-316.

Bailard, J. A., 1981. An energetics total load sediment transport model for a plane sloping beach. J. Geophysical Research, 86(C11): 10938-10954.

Brampton, A. H., Gilbert, G. and Southgate, H. N., 1984. A finite difference wave refraction model. HR Wallingford Report EX 1163, Wallingford, Oxon, UK. 15pp.

Christoffersen, J. E. and Jonsson, I. G., 1985. Bed friction and dissipation in a combined current and wave motion. Ocean Engineering, 12(5): 387-423.

Davies, A. G., Soulsby, R. L. and King, H. L., 1988. A numerical model of the combined wave and current bottom boundary layer. J. Geophysical Research, 93(C1): 491-508.

Fredsøe, J., 1984. Turbulent boundary layer in wave-current motion. J. Hydraul. Eng, ASCE, 110: 1103-1120.

Grant, W. D. and Madsen, O. S., 1979. Combined wave and current interaction with a rough bottom. J. Geophysical Research, 84(C4): 1797-1808.

HR Wallingford, 1991. Norfolk Sand Banks: Analysis of STABLE data (Part 1: Methods; Part 2: Results). HR Wallingford report EX 2345, Wallingford, Oxon. UK. November 1991.

Huynh-Thanh, S. and Temperville, A., 1991. A numerical model of the rough turbulent boundary layer in combined wave and current interaction. In: Sand Transport in Rivers, Estuaries and the Sea; Ed. R. L. Soulsby and R. Bettess; Pub. Balkema, Rotterdam. pp93-100.

Madsen, O. S., Poon, Y-K., and Graber, H. C., 1988. Spectral wave attenuation by bottom friction: Theory. Proceedings of the 21st International Conference on Coastal Engineering, Malaga, ASCE. Chapter 34, pp492-504.

Myrhaug. D. and Slaattelid, O. H., 1990. A rational approach to wave-current friction coefficients for rough, smooth and transitional turbulent flow. Coastal Engineering, 14: 265-293.

Simons, R. R., Grass, A. J. and Mansour-Tehrani, M., 1992. Bottom shear stresses in the boundary layer under waves and currents crossing at right angles. Proceedings of the 23rd International Conference on Coastal Engineering, Venice, ASCE Chapter 45, pp604-617.

Soulsby, R. L., 1993. Manual of Marine Sands. HR Wallingford Report SR 351, Wallingford, Oxon., UK.

Soulsby, R. L. and Humphery, J. D., 1989. Field Observations of wave-current interaction at the sea bed. Proceedings of NATO Advanced Research

Workshop on Water Wave Kinematics, ed. A. Tørum, Molde, Norway; pub. Kluwer Academic Pub., B.V., Dordrecht, Netherlands.

Soulsby, R. L., Hamm, L., Klopman, G., Myrhaug, D., Simons, R. R. and Thomas, G. P., 1993. Wave-Current Interaction within and outside the bottom boundary layer. Coastal Engineering, MAST G6M Special Issue (in press).

Swart, D. H., 1974. Offshore sediment transport and equilibrium beach profiles. Delft Hydraulics Laboratory. Publication 131.

Tucker, M. J., 1991. Waves in Ocean Engineering: measurement, analysis, interpretation. Ellis Horwood Series in Marine Science, Ed. T. D. Allan, Pub. Ellis Horwood Limited, Chichester, UK.

Zhao, Y. and Anastasiou, K., 1993. Bottom friction effects in the combined flow field of random waves and currents. Coastal Engineering, 19: 223-243.

Zyserman, J. A. and Fredsøe, J., 1988. Numerical simulation of concentration profiles of suspended sediment under irregular waves. Institute of Hydrodynamics and Hydraulic Engineering, Technical University of Denmark. Progress report 68, pp15-26.

Tables

Table 1 Summary of main flow variables at a height of 0.10m for STABLE Isle of Wight data

Burst	Mean current m/s	U_{rms} m/s	T_p s	Angle of waves to current °	σ_{wave} m/s	τ_m (obs) Nm^{-2}	τ_m (irreg) Nm^{-2}	$10^6 q_{irreg}$ m^2s^{-1}	$10^6 q_{reg}$ m^2s^{-1}
4	0.062	0.061	13.6	34.4	0.057	0.05	0.05	0.21	0.32
5	0.264	0.091	12.4	53.8	0.050	0.94	0.64	11.0	11.0
9	0.286	0.081	11.9	53.2	0.043	0.82	0.75	15.0	12.0
10	0.108	0.050	11.6	56.1	0.041	0.14	0.11	0.39	0.44
13	0.239	0.062	10.7	50.5	0.028	0.50	0.51	7.40	6.40
14	0.214	0.064	13.7	64.7	0.035	0.45	0.39	4.40	3.90
17	0.219	0.074	13.6	53.7	0.051	0.42	0.43	5.50	5.40
18	0.279	0.087	13.8	66.3	0.057	0.62	0.69	12.0	11.0
21	0.114	0.062	13.0	41.7	0.056	0.15	0.15	1.00	0.98
22	0.371	0.111	12.8	61.1	0.072	0.90	1.19	31.0	28.0
25	0.055	0.065	11.8	12.9	0.063	0.04	0.06	0.72	0.40
26	0.432	0.110	10.7	52.1	0.067	1.24	1.59	49.0	45.0
27	0.025	0.068	12.4	125.2	0.068	0.03	0.01	0.14	0.07
30	0.440	0.108	11.2	50.3	0.046	1.51	1.63	51.0	47.0
31	0.136	0.067	9.9	68.1	0.054	0.18	0.19	1.60	1.10
34	0.459	0.163	14.2	72.2	0.121	1.74	1.83	60.0	57.0
35	0.211	0.089	15.6	73.0	0.072	0.31	0.40	4.80	4.50
38	0.459	0.116	14.3	60.2	0.077	1.34	1.72	52.0	51.0
39	0.290	0.089	14.1	68.4	0.057	0.71	0.72	13.0	12.0
42	0.390	0.101	13.3	46.5	0.038	1.27	1.34	37.0	33.0
43	0.381	0.095	12.6	46.3	0.046	1.03	1.27	34.0	31.0
46	0.331	0.081	10.1	65.1	0.018	0.92	0.93	20.0	18.0
47	0.418	0.101	12.2	65.7	0.032	1.36	1.44	40.0	37.0
54	0.209	0.062	11.6	35.8	0.033	0.38	0.42	5.50	4.90
55	0.504	0.123	10.7	48.8	0.063	2.25	2.17	77.0	73.0
58	0.154	0.079	5.9	28.3	0.071	0.20	0.25	2.70	4.20
59	0.425	0.171	7.7	50.1	0.098	4.77	1.76	65.0	60.0
62	0.035	0.117	7.6	-9.5	0.118	0.14	0.03	0.43	0.64

Table 2 Summary of main flow variables at a height of 0.41m for STABLE Norfolk Sand Banks data

Burst	Mean current ξ m/s	U_{rms} m/s	T_p s	Angle of waves to current °	σ_{wave} m/s	τ_m (obs) Nm^{-2}	τ_m (irreg) Nm^{-2}	$10^6 q_{irreg}$ m^2s^{-1}	$10^6 q_{reg}$ m^2s^{-1}
1	0.486	0.193	9.1	131.2	0.173	2.85	0.94	24.0	26.0
2	0.610	0.207	9.5	154.3	0.159	4.77	1.60	56.0	56.0
3	0.284	0.168	9.1	174.6	0.158	1.13	0.41	6.7	10.0
4	0.171	0.165	10.6	-57.6	0.152	1.42	0.17	2.3	2.2
5	0.450	0.155	11.0	-33.4	0.119	1.95	0.87	21.0	21.0
6	0.244	0.146	10.6	-22.1	0.132	0.87	0.32	4.6	5.8
7	0.211	0.119	10.3	140.3	0.109	0.72	0.23	2.8	2.7
8	0.480	0.173	10.5	154.0	0.139	2.65	0.99	25.0	28.0
9	0.220	0.142	10.7	170.7	0.127	0.66	0.27	3.9	4.9
10	0.321	0.140	10.7	-39.1	0.125	0.79	0.42	6.1	8.3
11	0.614	0.164	10.8	-35.4	0.108	1.93	1.47	45.0	44.0
12	0.517	0.178	11.0	-24.0	0.133	1.76	1.19	36.0	34.0
13	0.130	0.148	10.9	78.7	0.149	0.28	0.09	1.1	0.8
14	0.600	0.200	8.6	152.6	0.159	2.41	1.50	50.0	52.0
15	0.557	0.197	10.7	163.8	0.164	2.46	1.37	43.0	45.0
16	0.077	0.185	10.9	257.3	0.183	0.48	0.04	0.94	0.52
17	0.411	0.170	10.1	-42.4	0.151	0.97	0.71	15.0	17.0
18	0.438	0.180	8.6	-29.0	0.158	1.01	0.84	20.0	24.0
19	0.151	0.145	10.0	100.1	0.146	0.25	0.11	1.1	1.0
20	0.599	0.204	8.5	164.2	0.170	2.53	1.59	57.0	57.0
21	0.457	0.209	9.9	161.0	0.198	1.46	1.02	30.0	31.0
22	0.111	0.202	11.1	-63.7	0.200	0.69	0.08	0.62	1.4
23	0.472	0.189	12.1	-38.2	0.167	0.99	0.96	25.0	25.0
24	0.660	0.205	11.0	-30.7	0.160	1.76	1.81	65.0	63.0
25	0.260	0.170	11.1	-5.8	0.153	1.01	0.38	7.1	8.5
26	0.405	0.174	10.6	135.1	0.166	0.69	0.72	16.0	16.0
27	0.664	0.203	11.3	160.9	0.172	2.66	1.78	62.0	67.0

Figures

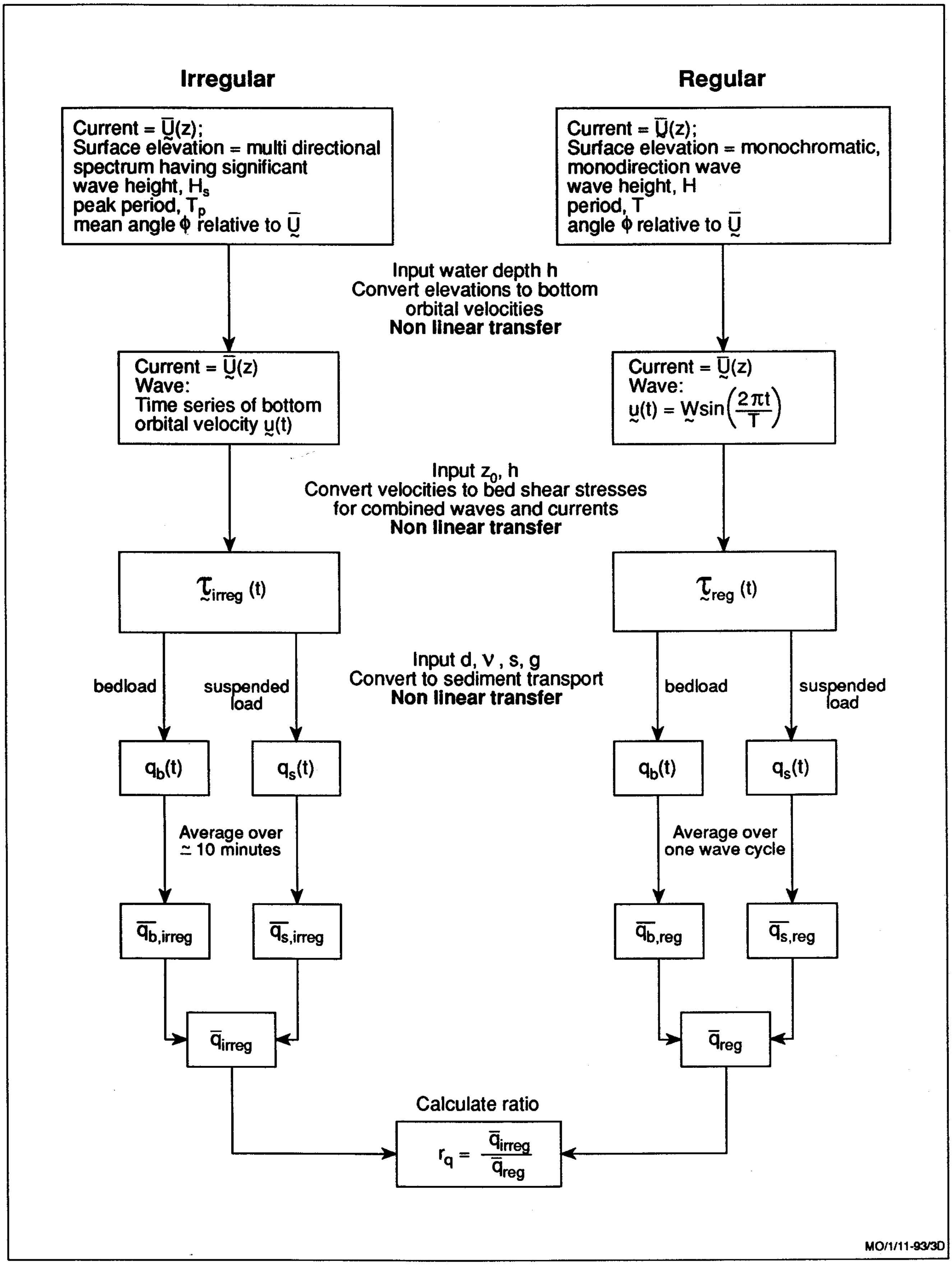

Figure 1 Method of approach for calculating sediment transport under irregular waves

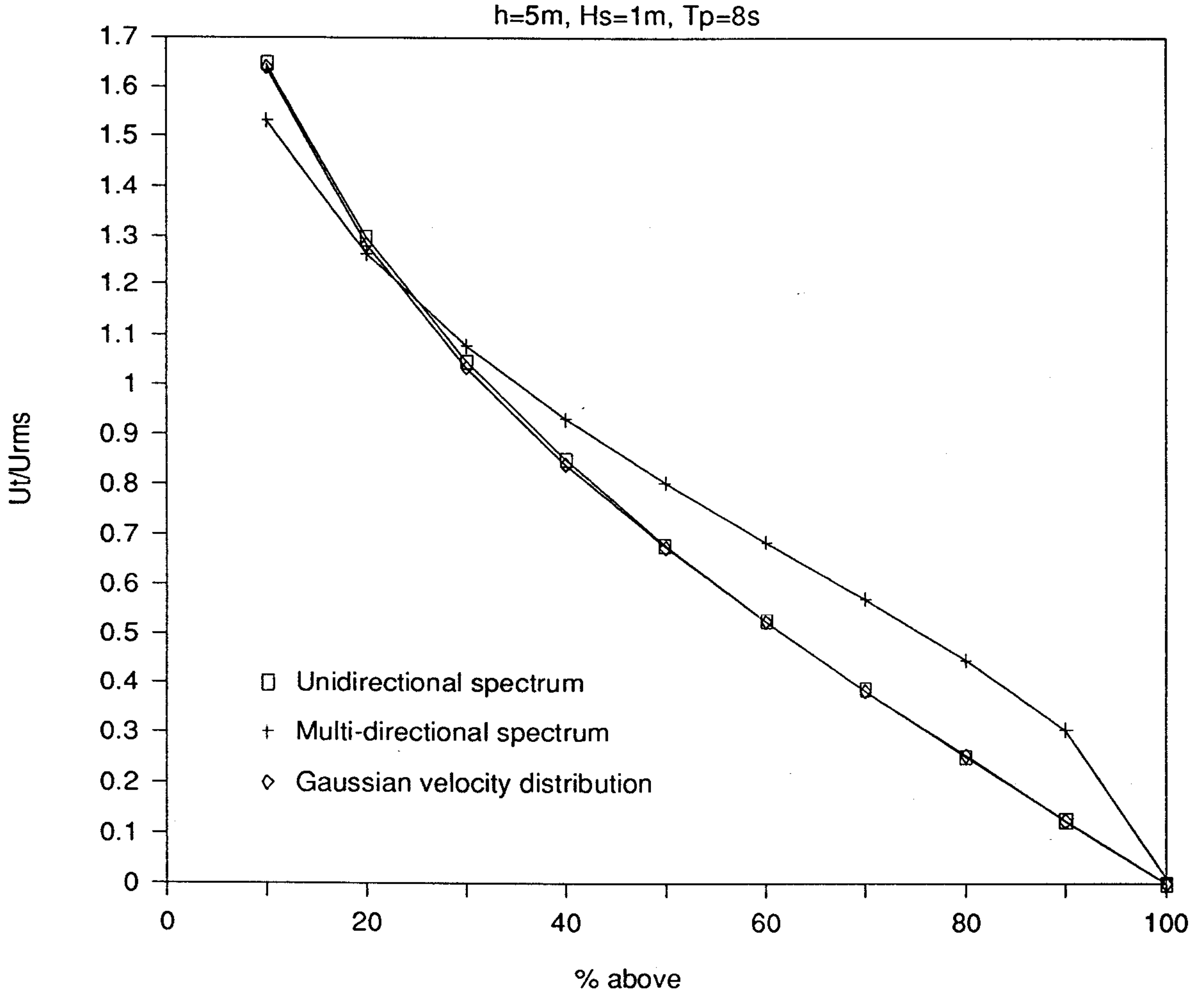

Figure 2 Percentage exceedence curves for U(t)/Urms, for unidirectional and multidirectional spectra

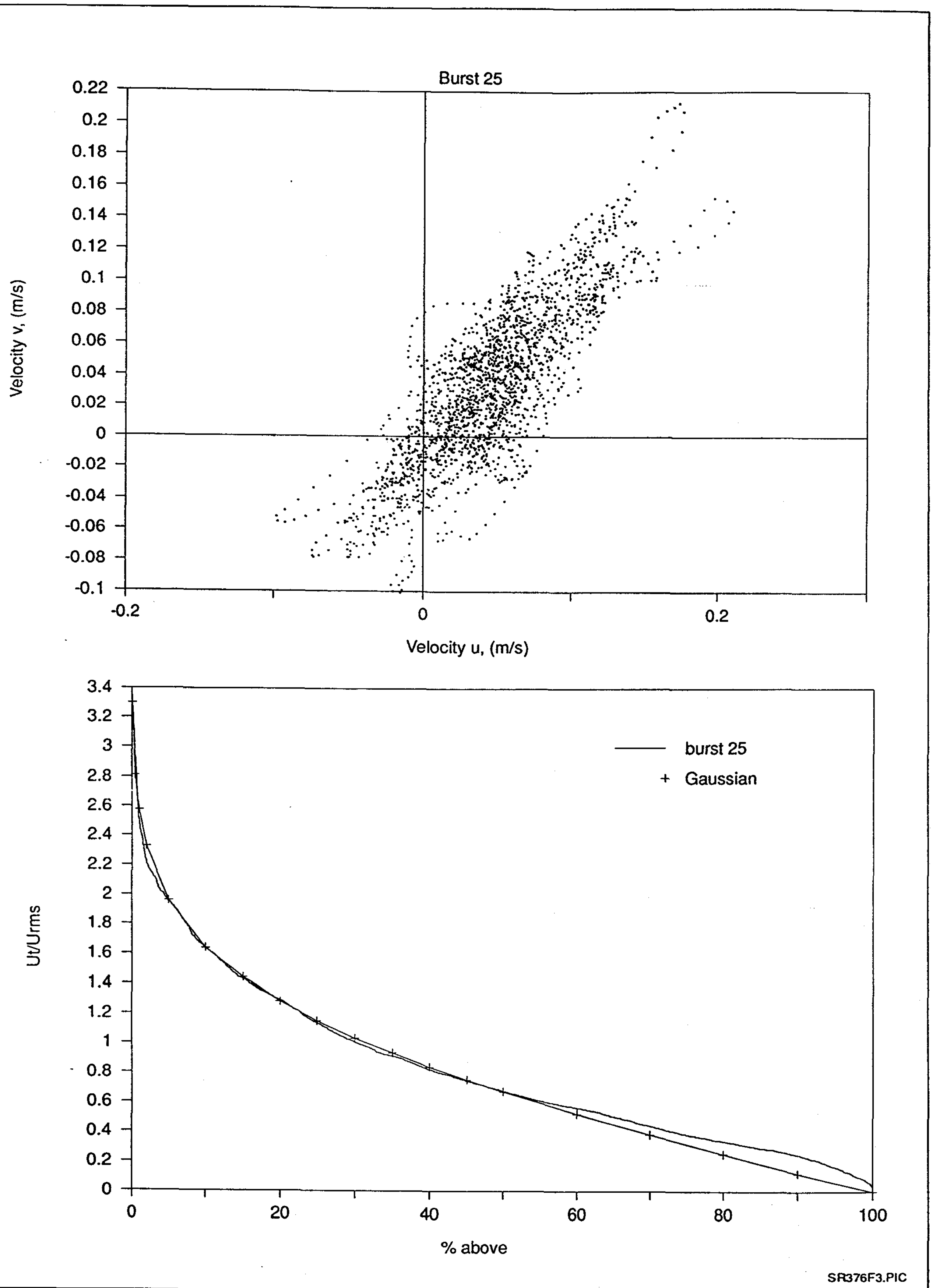

Figure 3 Scatter plot for velocities from Isle of Wight, burst 25; Percentage exceedence curve for U(t)/Urms, burst 25

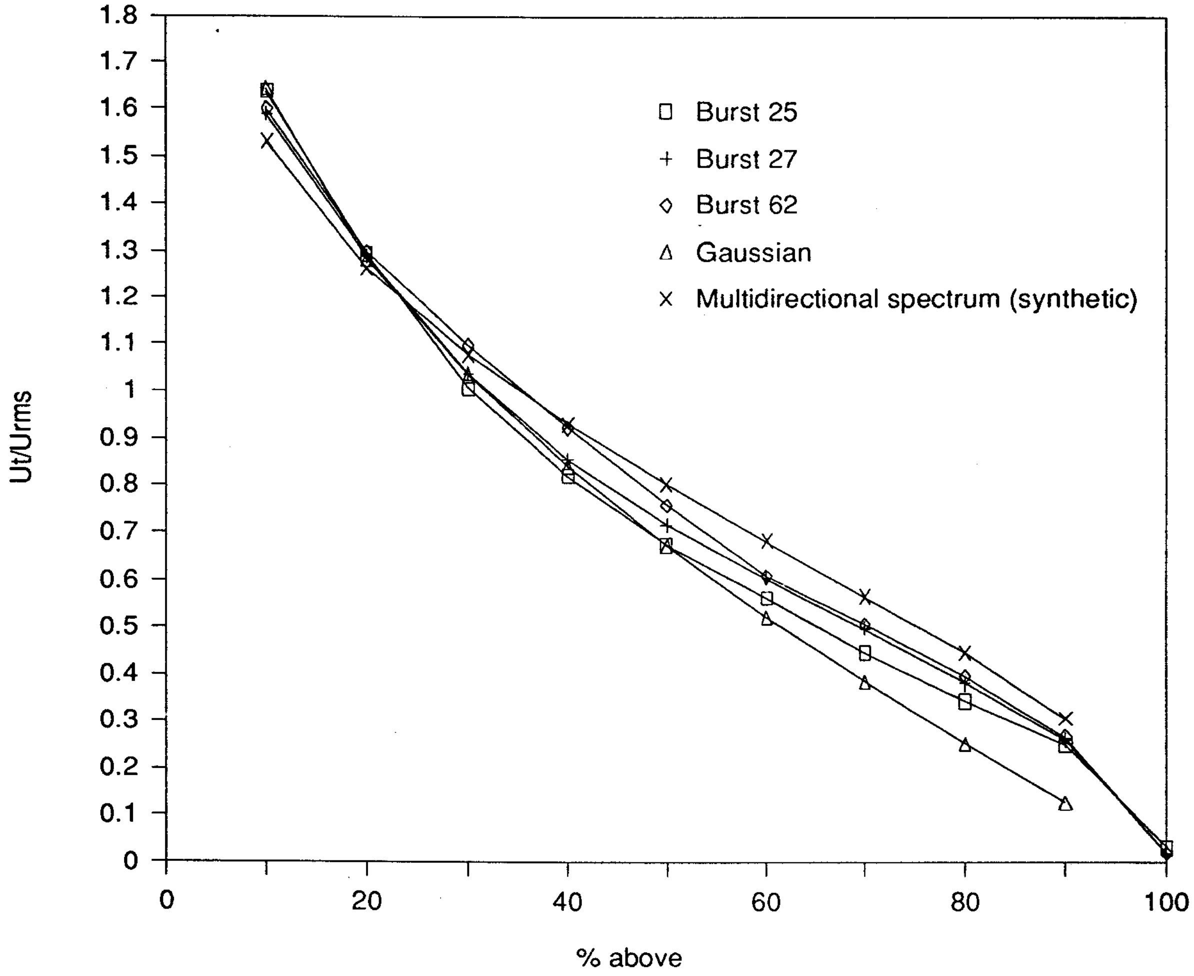

SR376F4.PIC

Figure 4 Percentage exceedence curves for U(t)/Urms, synthetic wave data and Isle of Wight bursts 25, 27 and 62

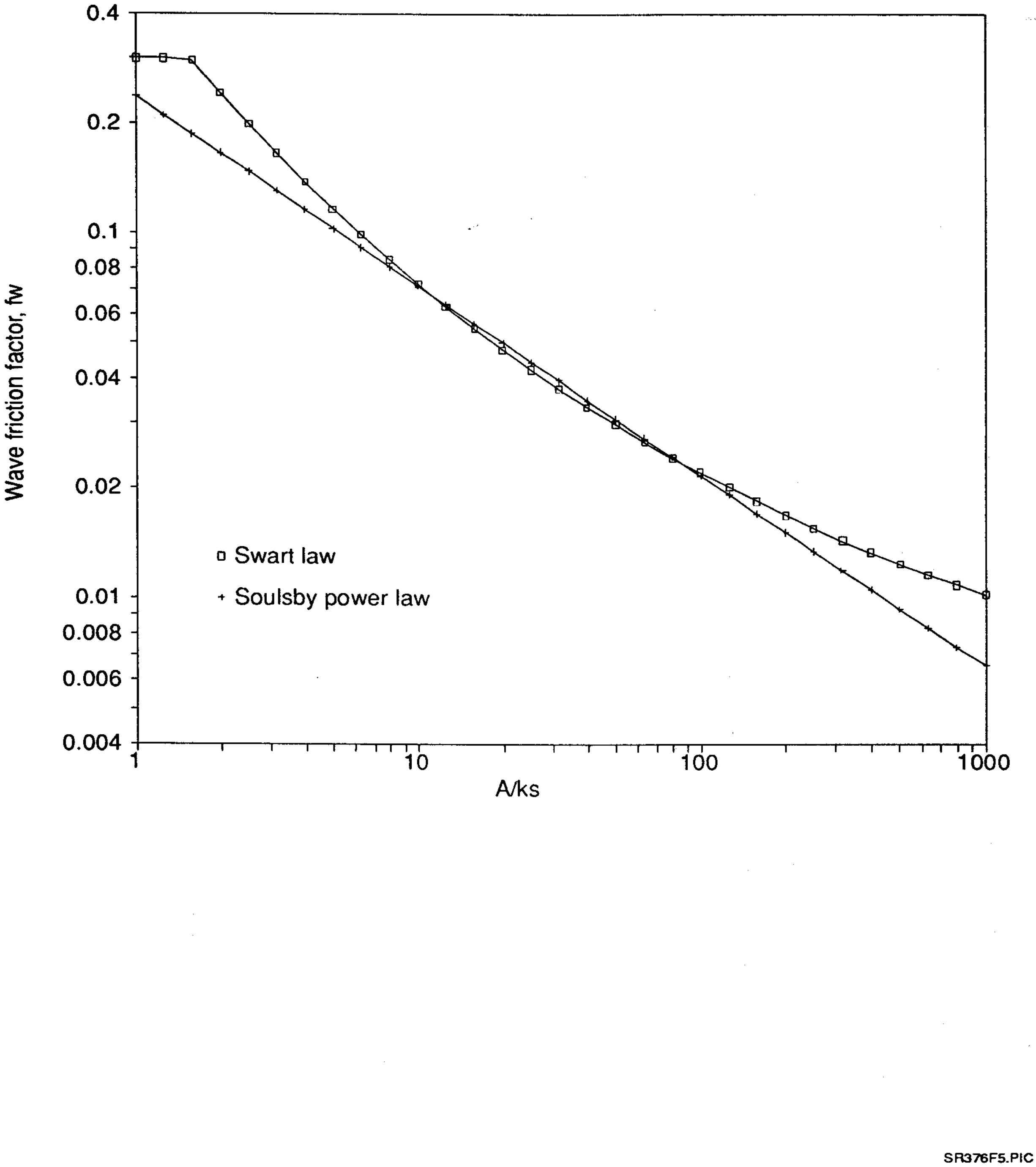

Figure 5 Wave friction factor calculated from Swart law and Soulsby power law

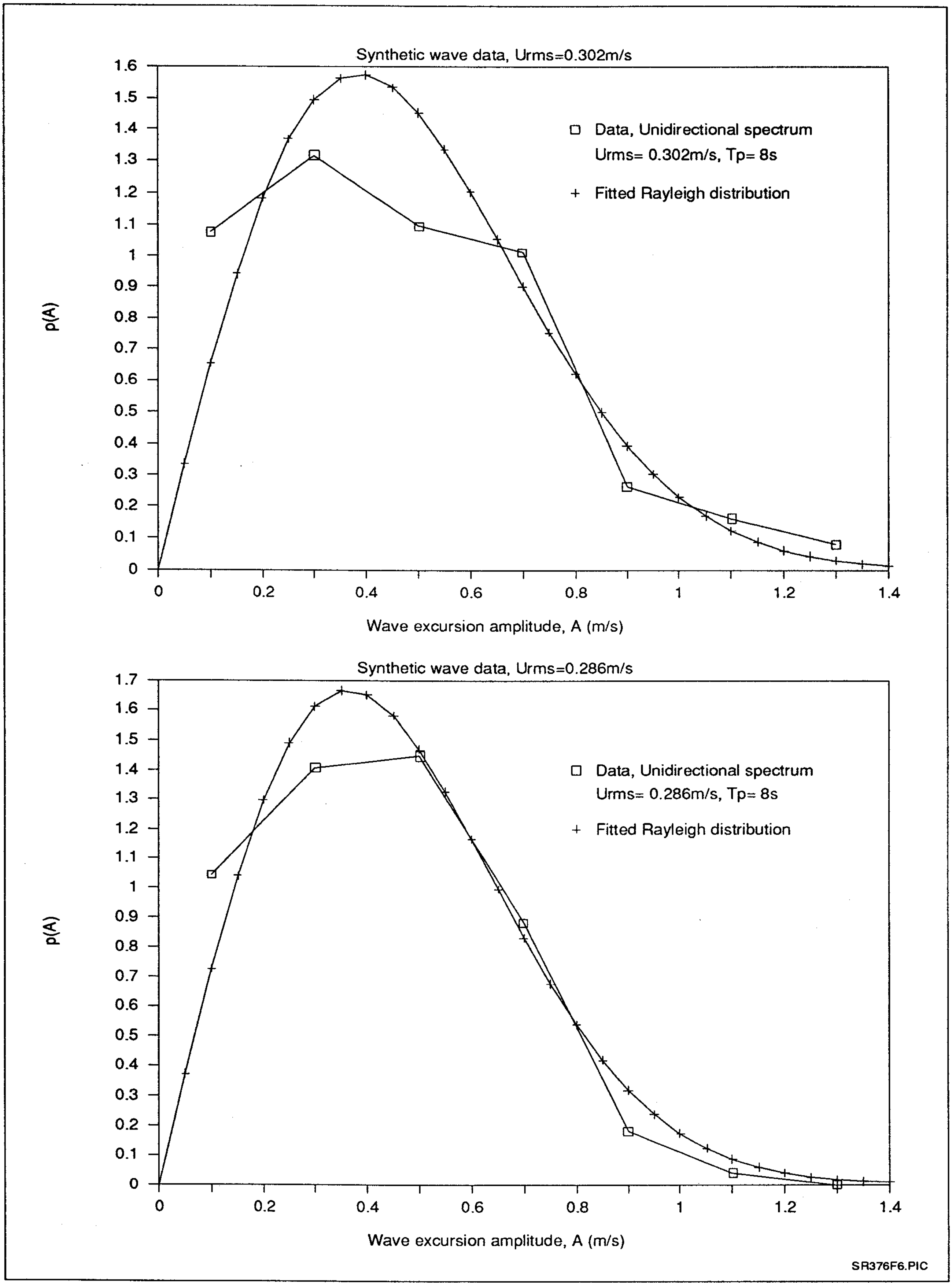

Figure 6 Distribution of wave excursion amplitude, A, calculated from synthetic wave data, with fitted Rayleigh distribution

Velocities:

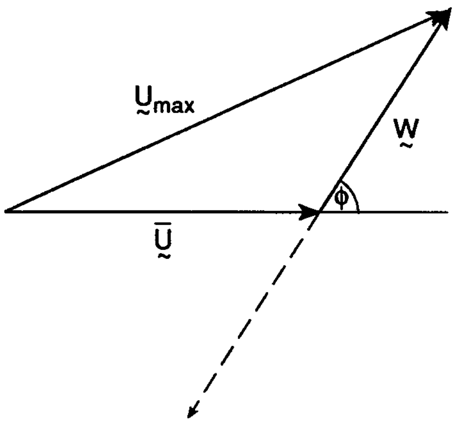

$\bar{\underset{\sim}{U}}$	=	mean current velocity
U_{rms}	=	root-mean-square of wave orbital velocity
W	=	$\sqrt{2}\, U_{rms}$
	=	maximum orbital velocity of sinusoidal wave with the same rms as irregular wave spectrum
$\underset{\sim}{U}_{max}$	=	maximum velocity of combined wave and current

Shear stresses:

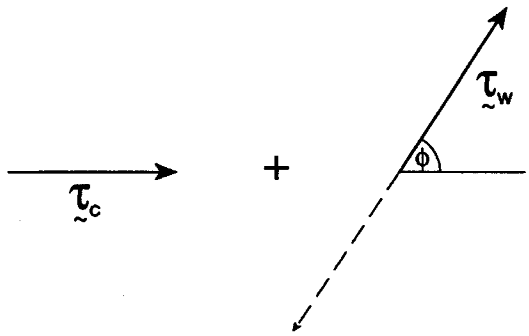

$\underset{\sim}{\tau}_c = \rho C_D |\bar{\underset{\sim}{U}}| \bar{\underset{\sim}{U}}$ (current only)

$\underset{\sim}{\tau}_w = \frac{1}{2}\, \rho f_w |\underset{\sim}{W}| \underset{\sim}{W}$ (wave only)

For combined waves and currents:

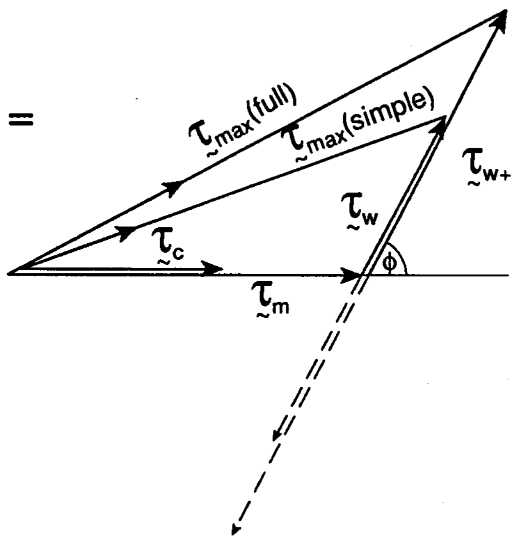

$\underset{\sim}{\tau}_m = \rho C_{D+} |\bar{\underset{\sim}{U}}| \bar{\underset{\sim}{U}}$

$\underset{\sim}{\tau}_{max}(\text{full}) = \underset{\sim}{\tau}_m + \underset{\sim}{\tau}_{w+}$

$\underset{\sim}{\tau}_{w+} = \frac{1}{2}\, \rho f_{w+} |\underset{\sim}{W}| \underset{\sim}{W}$

where τ_m and τ_{max} are calculated from G6M parameterised models

MO/8/11-93/3D

Figure 7 Definitions of velocity and shear stress vectors for wave, current and combined shear stresses

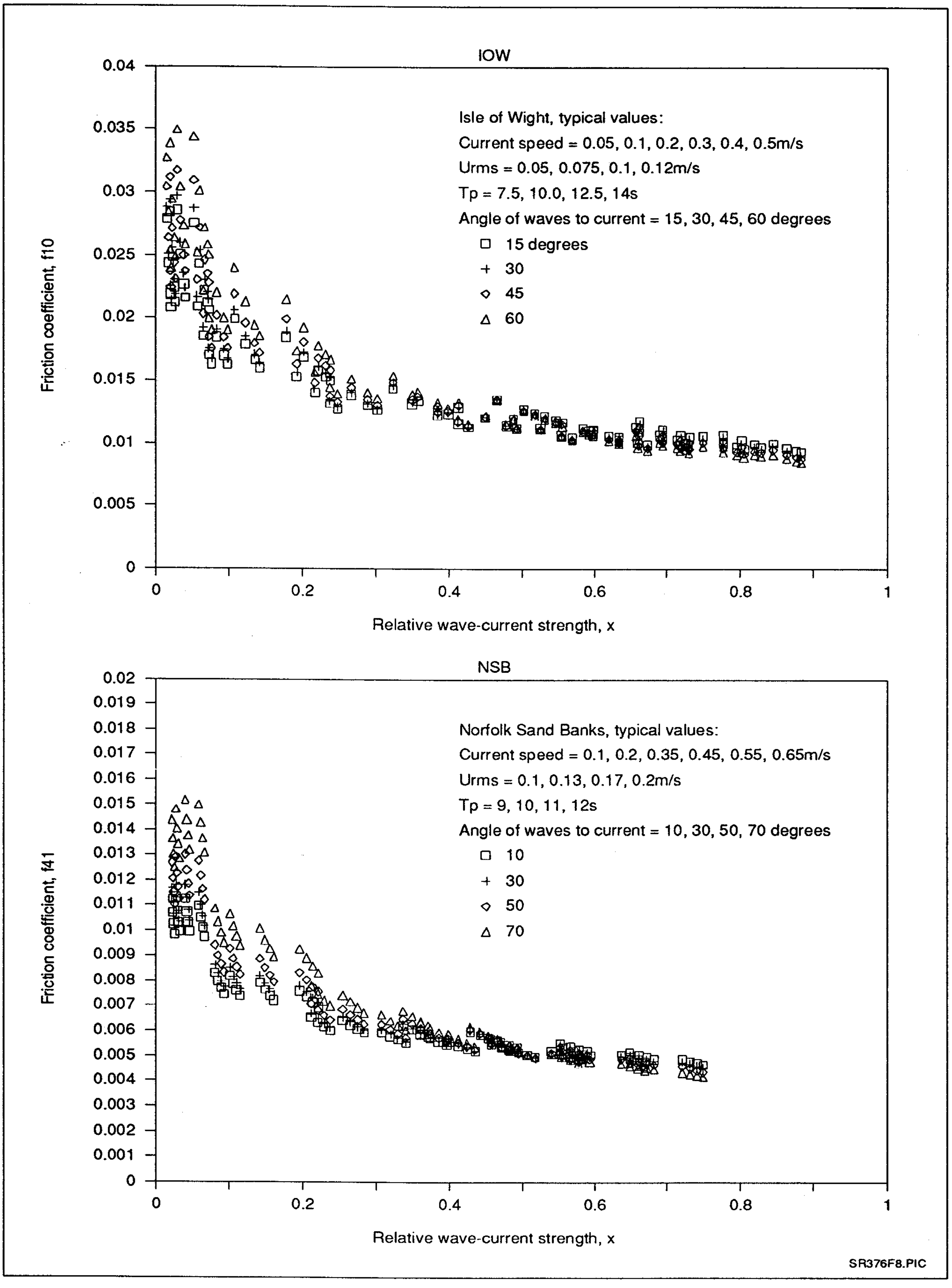

Figure 8 Friction coefficients for a combined wave and current shear stress calculated using typical values from IOW and NSB

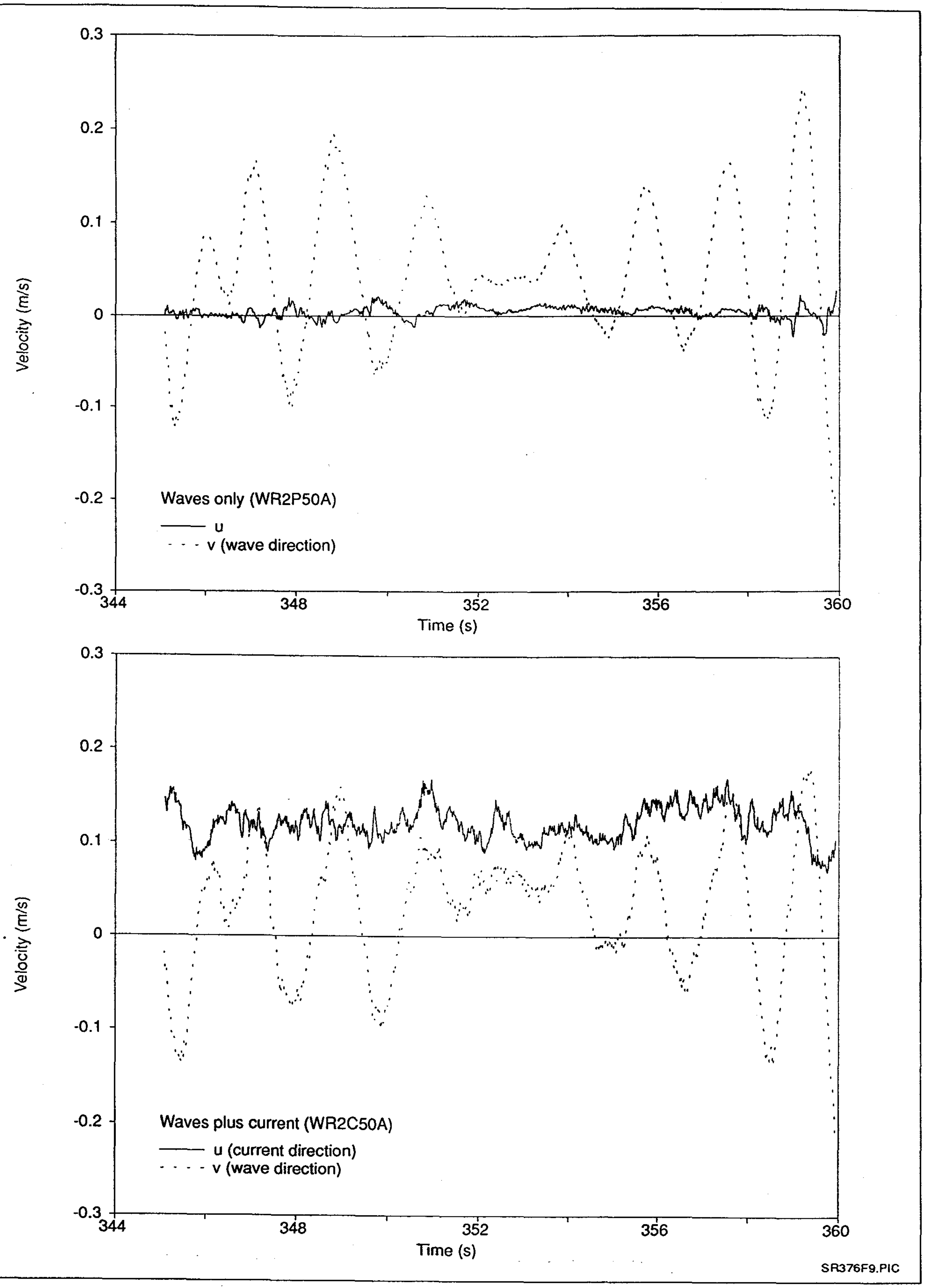

Figure 9 Wave and current velocities for UCL laboratory tests for wave only and corresponding wave plus current test

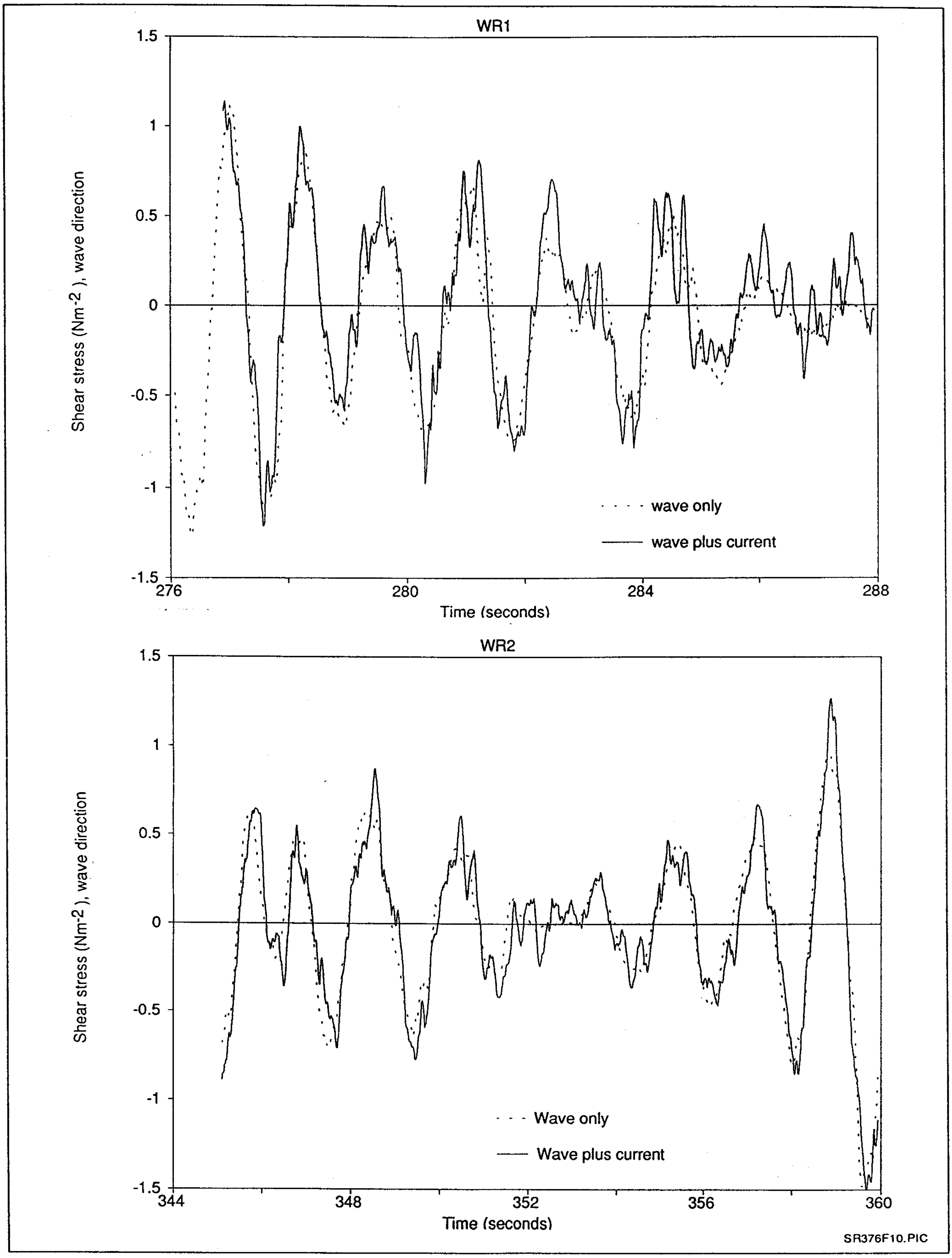

Figure 10 Shear stresses measured in UCL laboratory tests for wave only and corresponding wave plus current tests WR1 and WR2

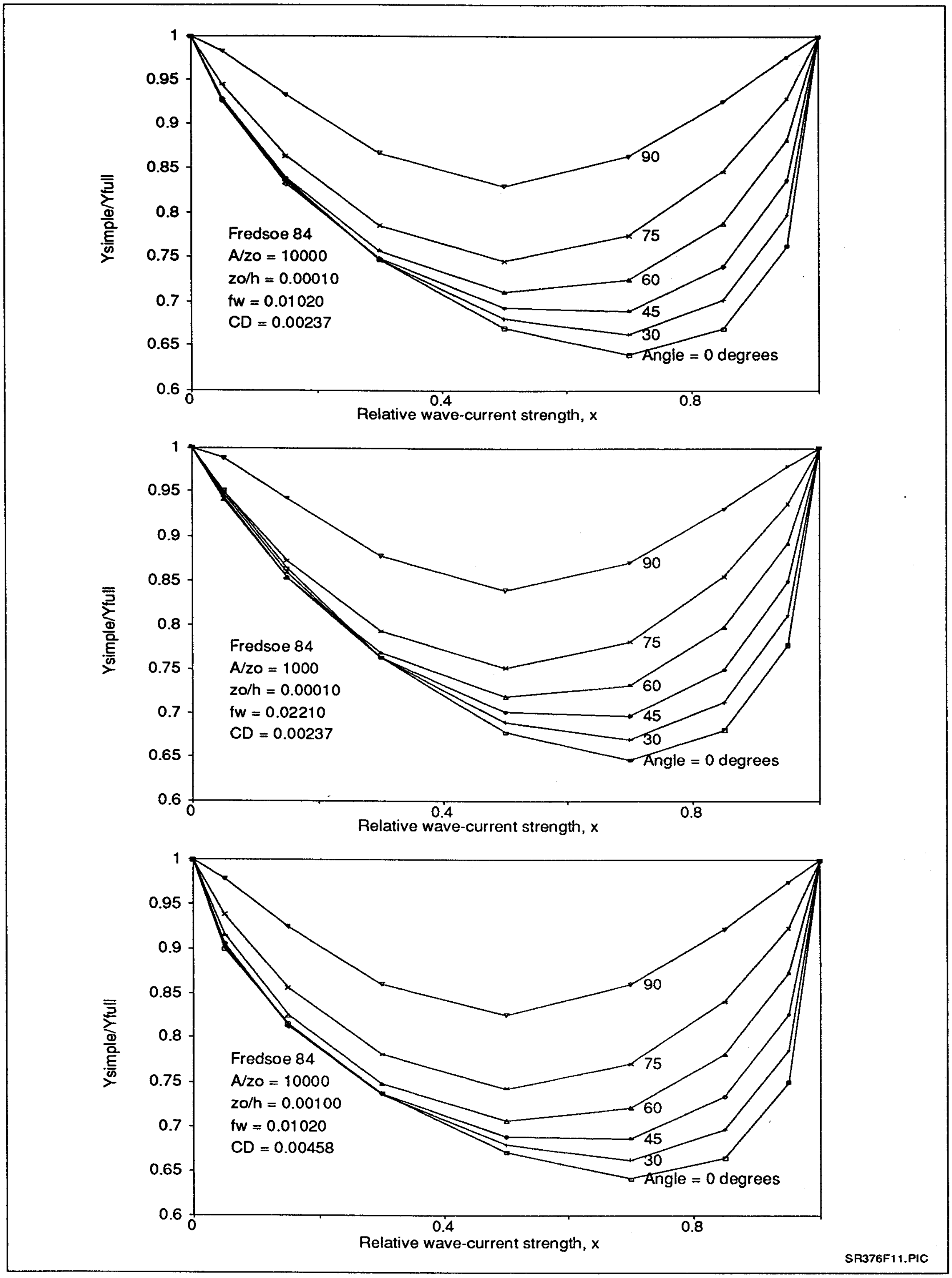

Figure 11 Ysimple/Yfull for Fredsoe 84 model, with variation in A/z0 and z0/h

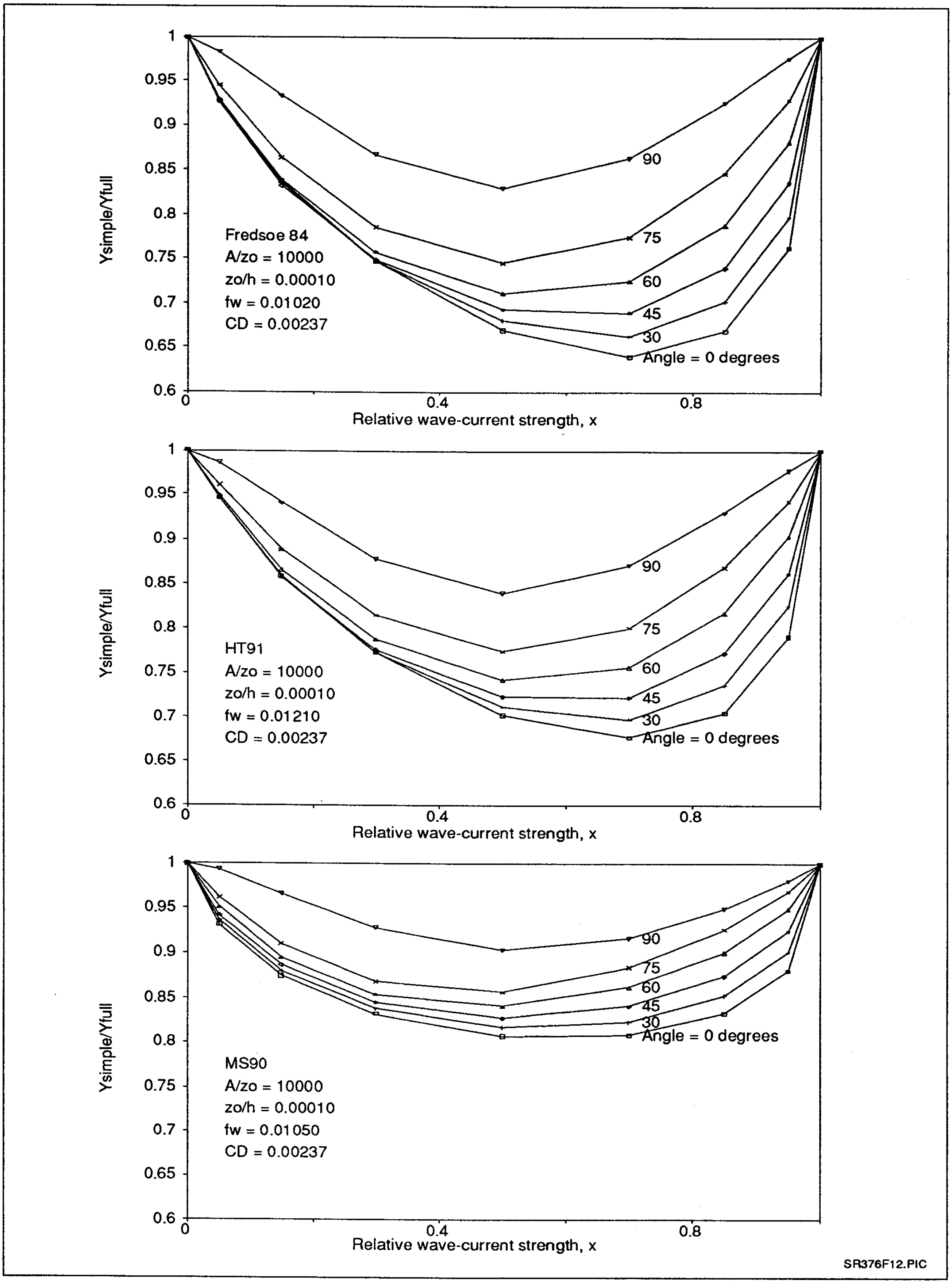

Figure 12 Ysimple/Yfull for Fredsoe 84, Huynh-Thanh and Temperville 1991 (HT91), Myrhaug and Slaattelid 1990 (MS90) models

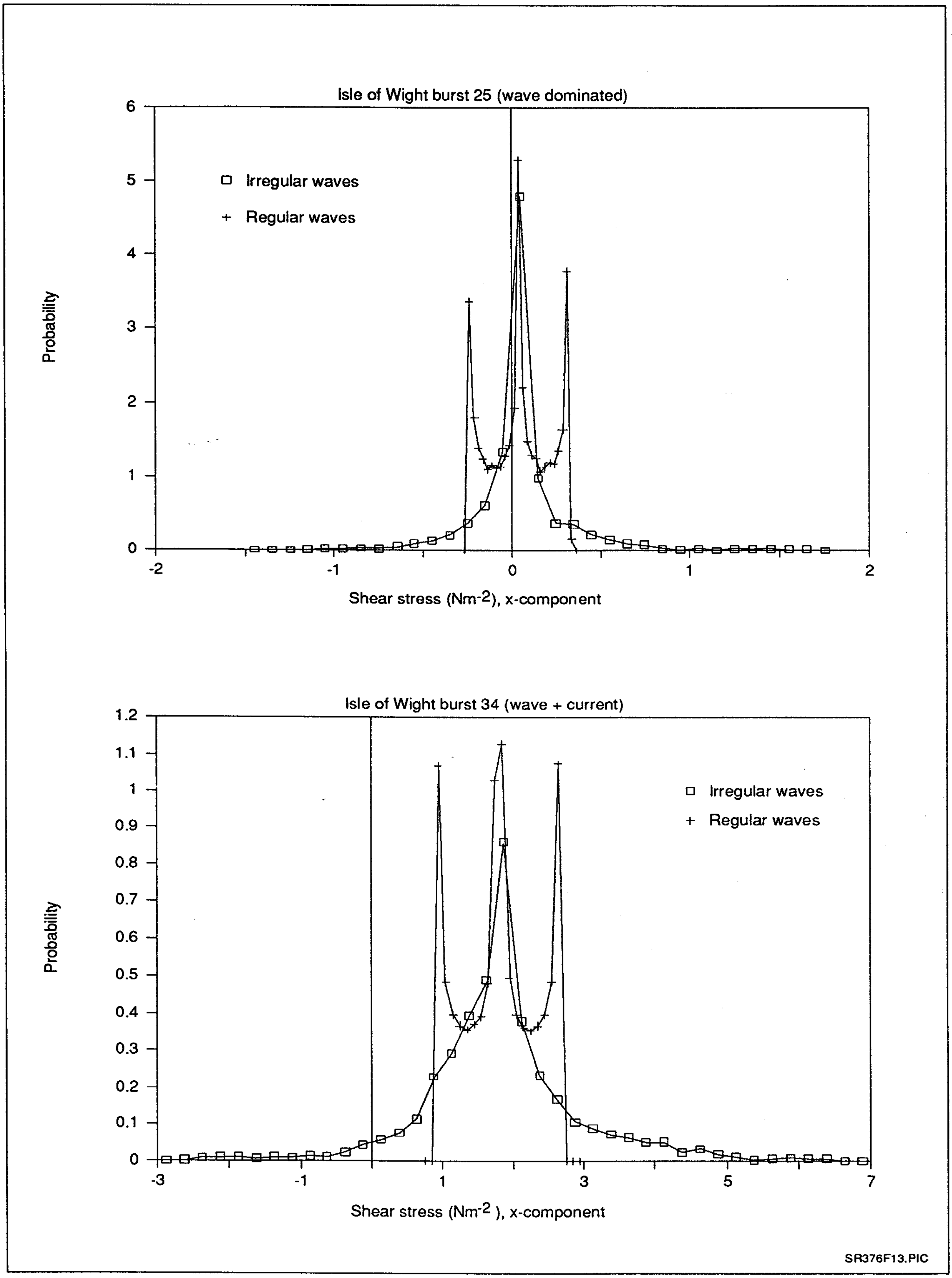

Figure 13 Probability distribution of shear stress for irregular and regular waves (x-component), from IOW bursts 25 and 34

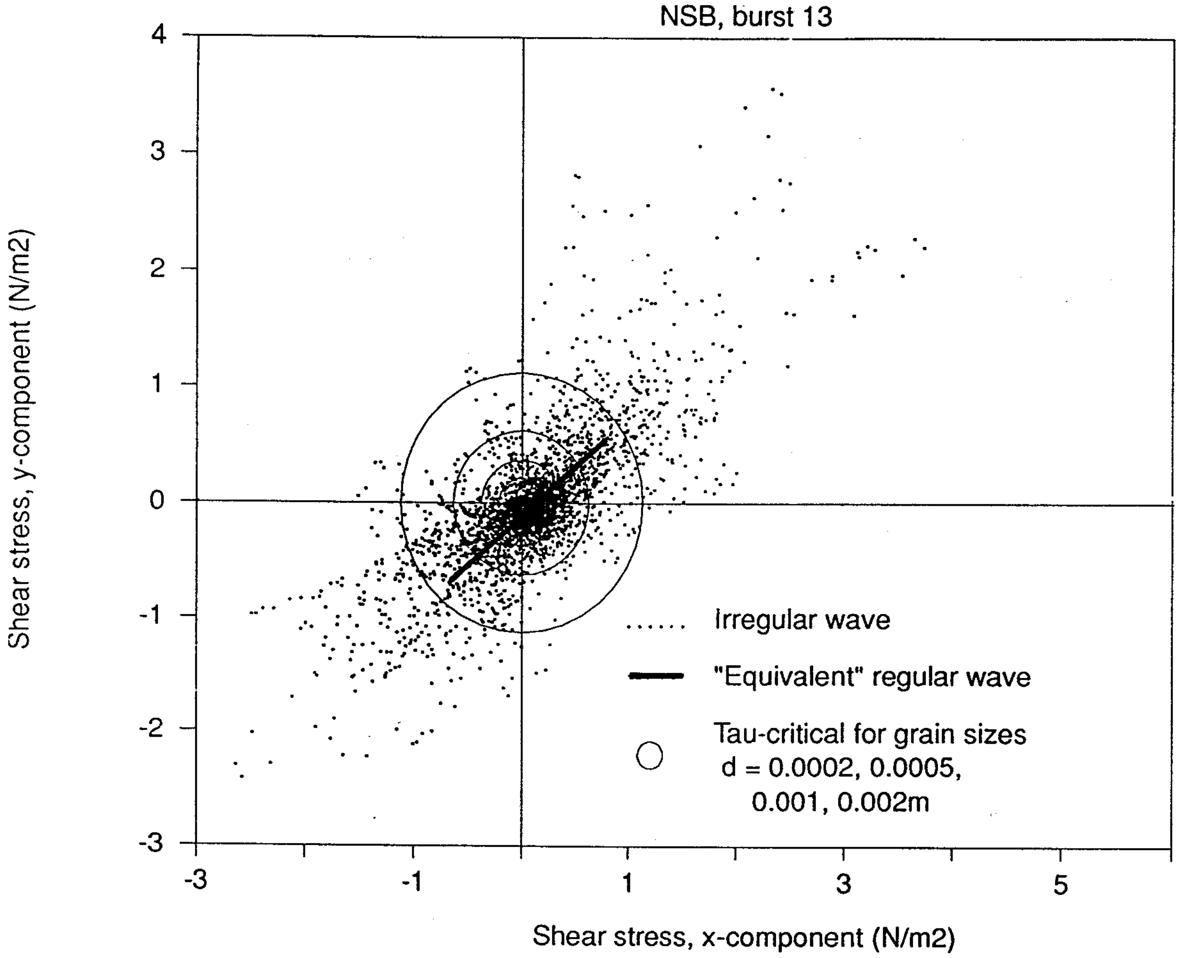

SR376F14.PIC

Figure 14 Irregular and regular shear stresses calculated for NSB burst 13 and "exclusion zone" for different thresholds of motion

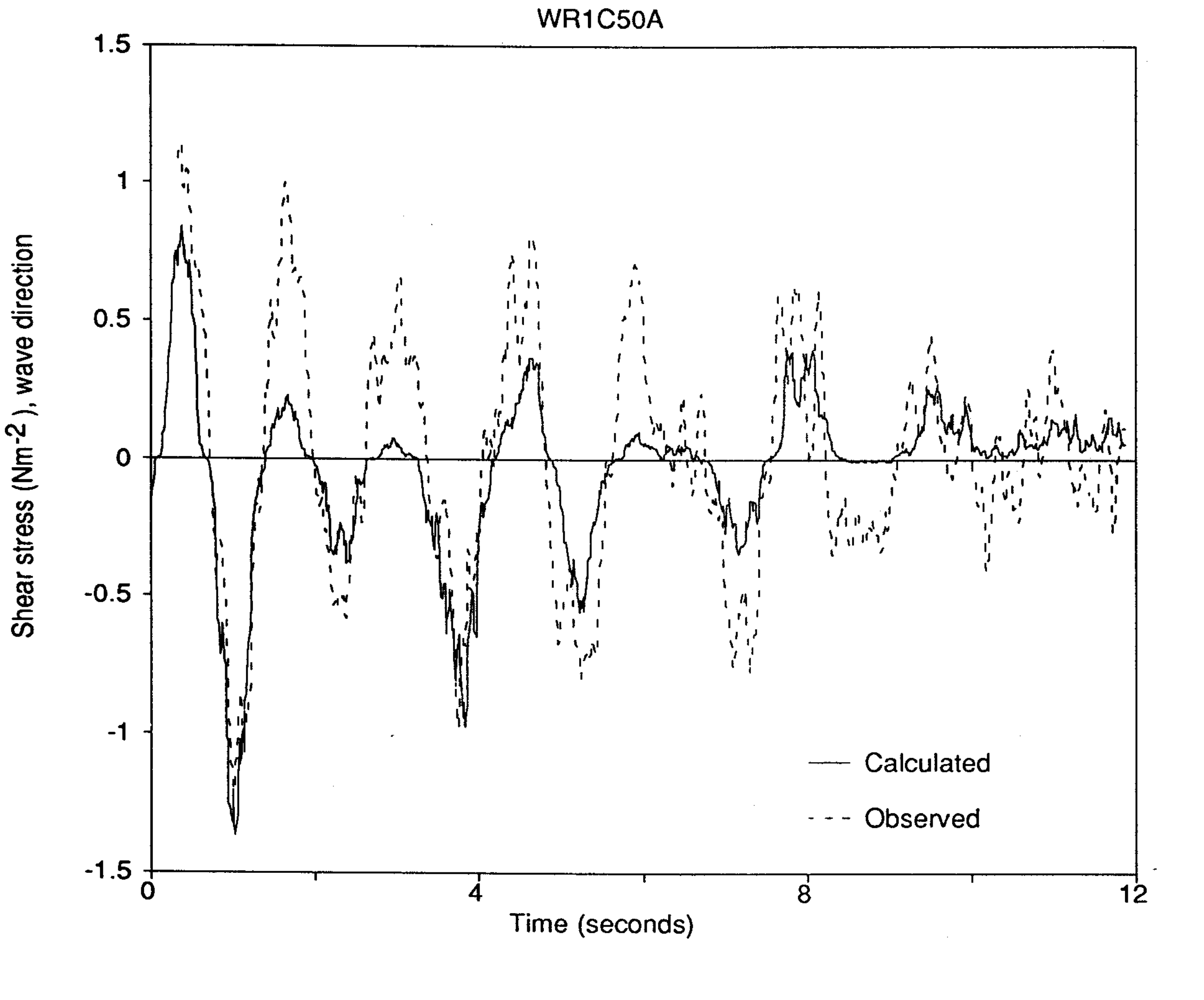

Figure 15 Comparison of shear stress from UCL laboratory tests with time series calculated according to Appendix 1

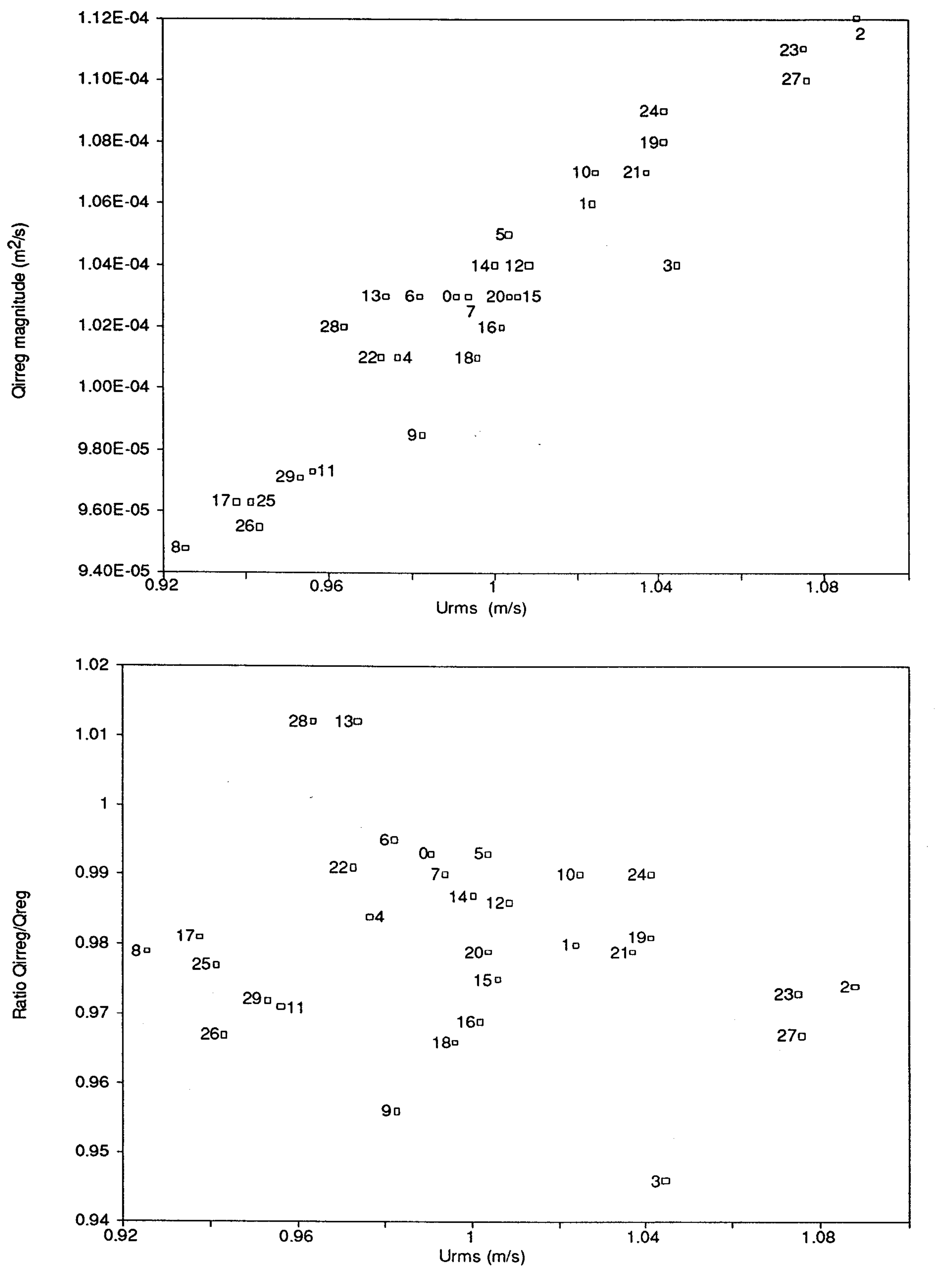

Figure 16 Statistical variation of mean sediment transport (magnitude and ratio irregular/regular) for synthetic wave data

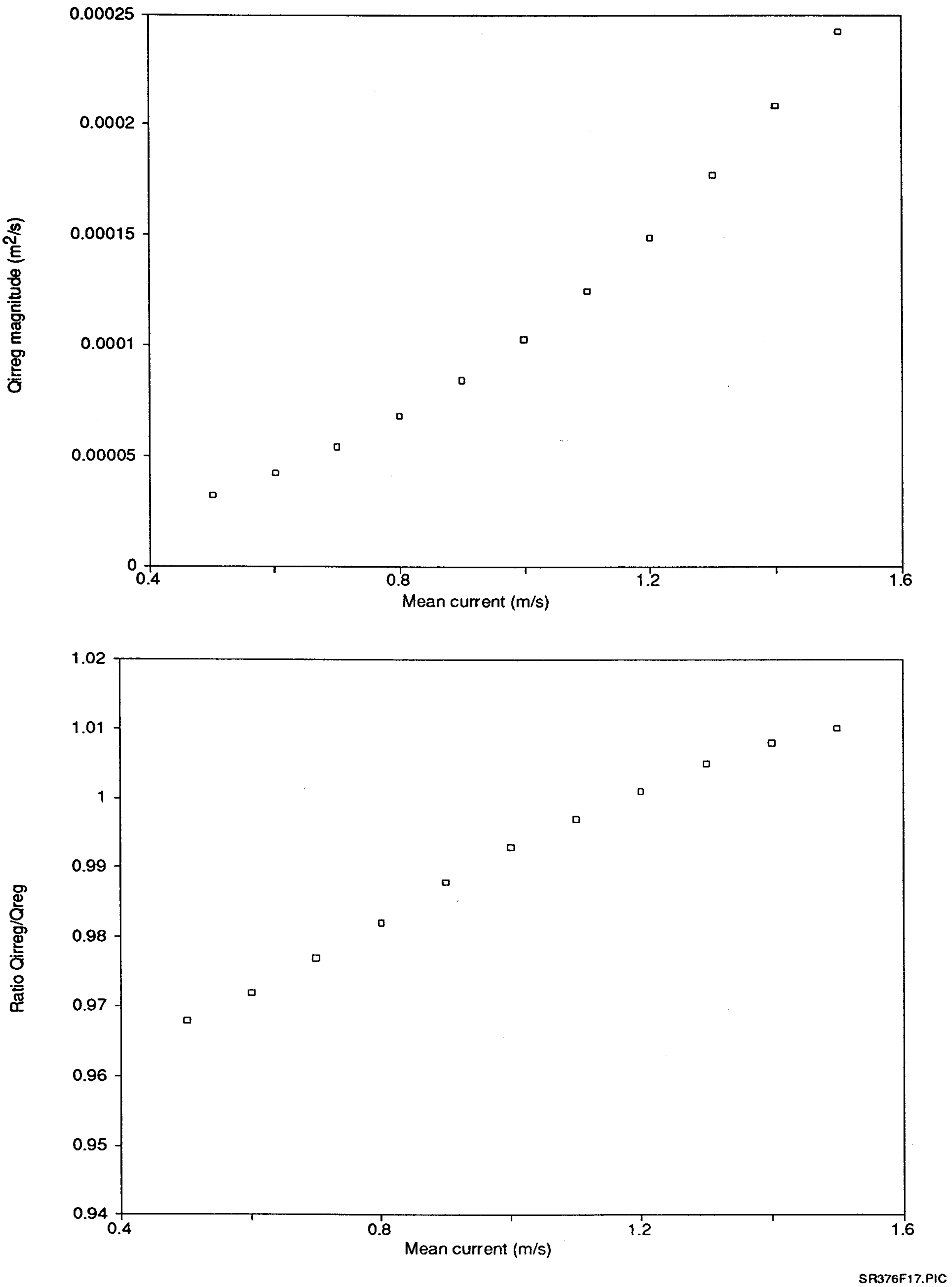

Figure 17 Variation of mean sediment transport (irregular/regular) with variation in mean current

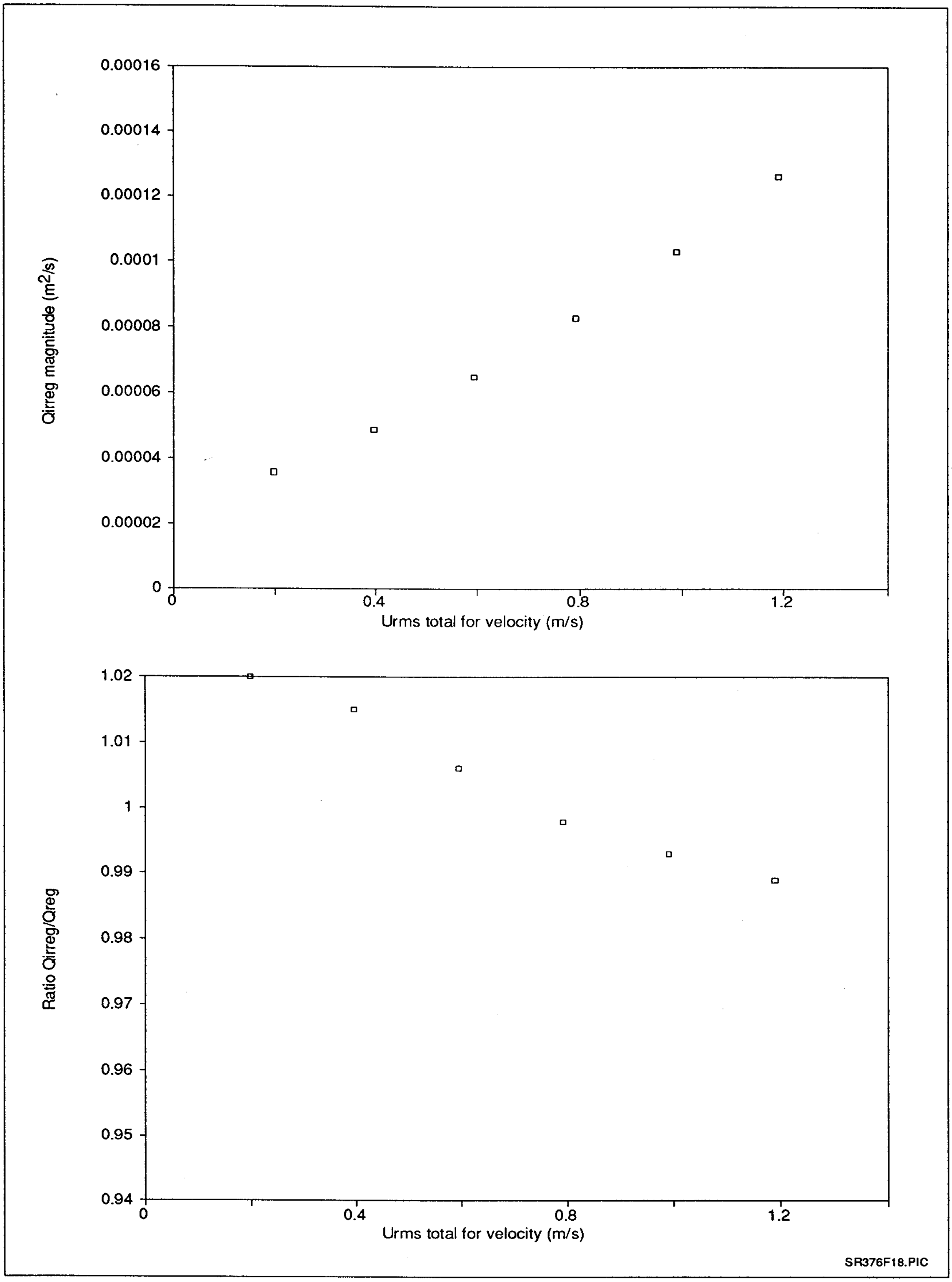

Figure 18 Variation of mean sediment transport (irregular/regular) with variation in wave orbital velocity

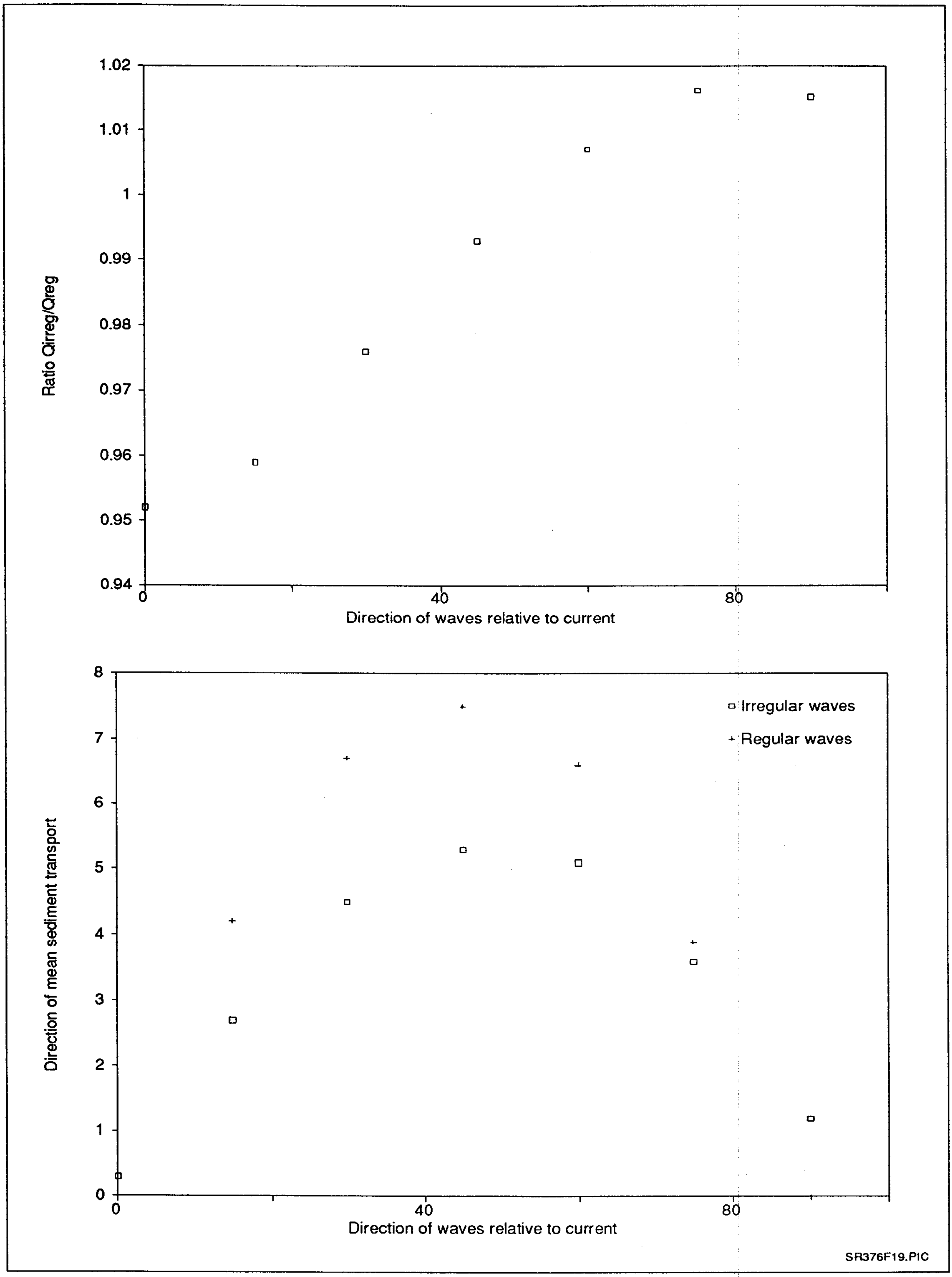

Figure 19 Variation of mean sediment transport (irregular/regular) with variation in direction of waves relative to current

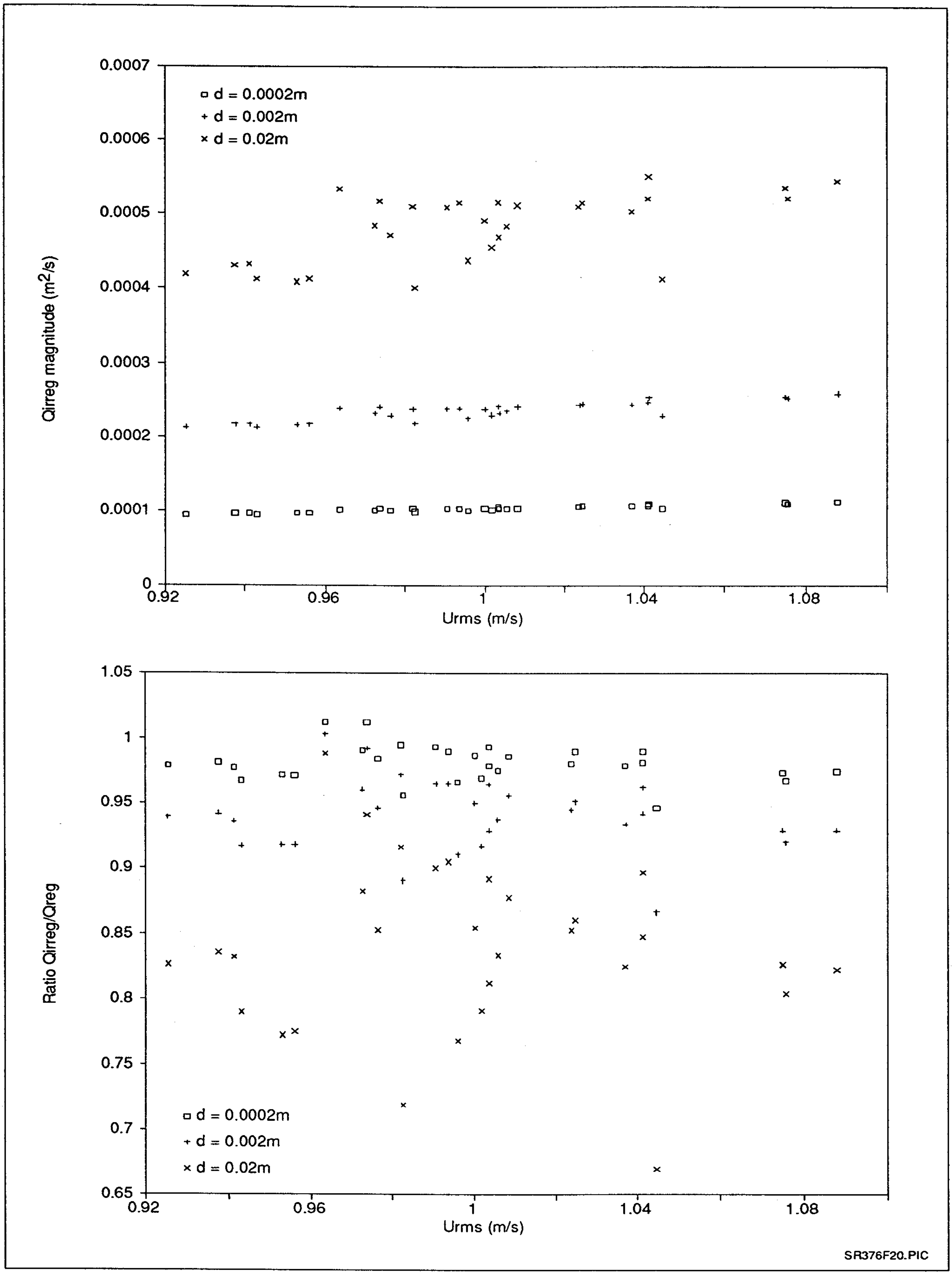

Figure 20 Variation of mean sediment transport (irregular/regular) with variation in grain size

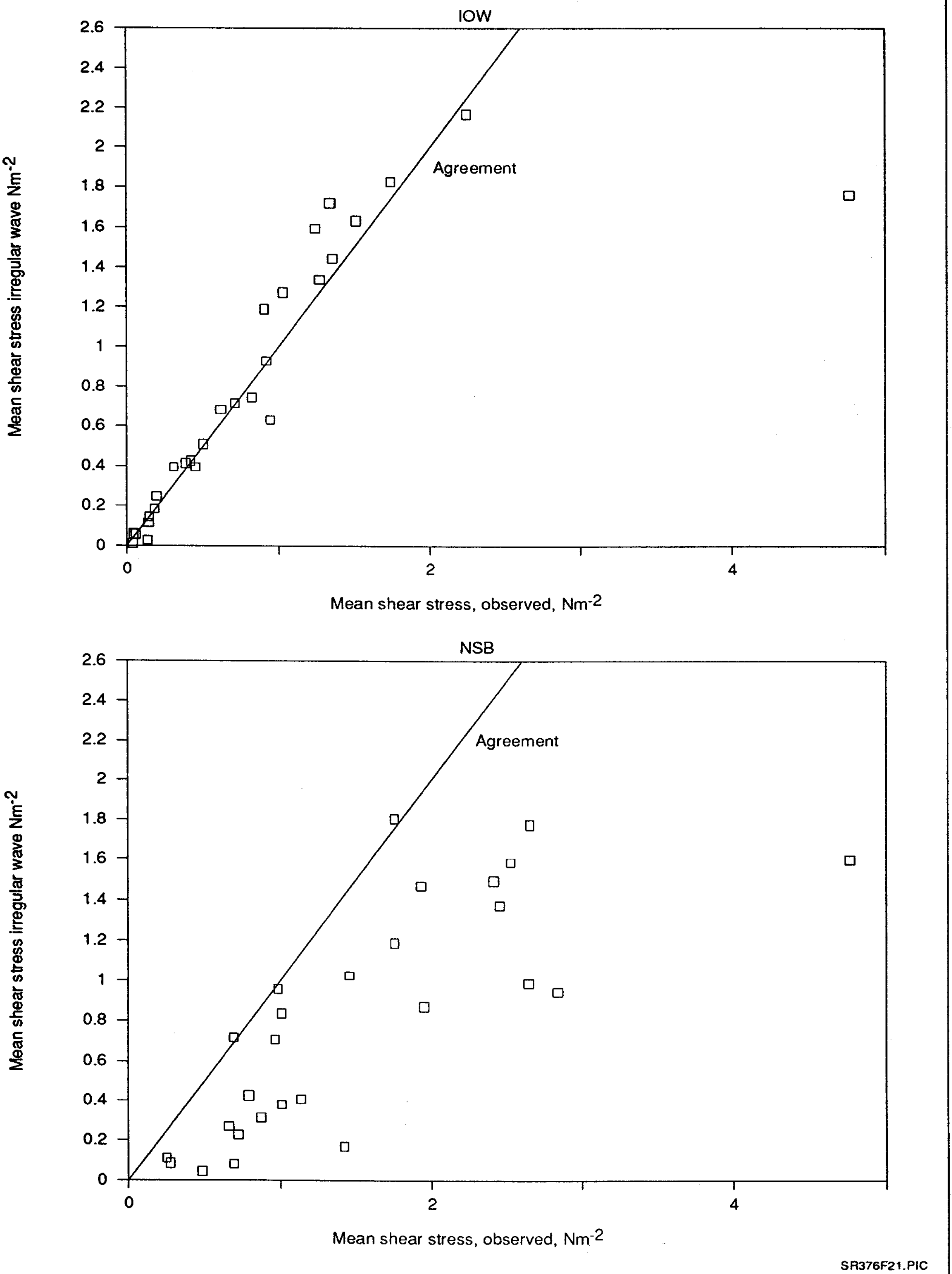

Figure 21 Mean shear stress (irregular wave) against mean shear stress (observed) for Isle of Wight and Norfolk Sand Banks

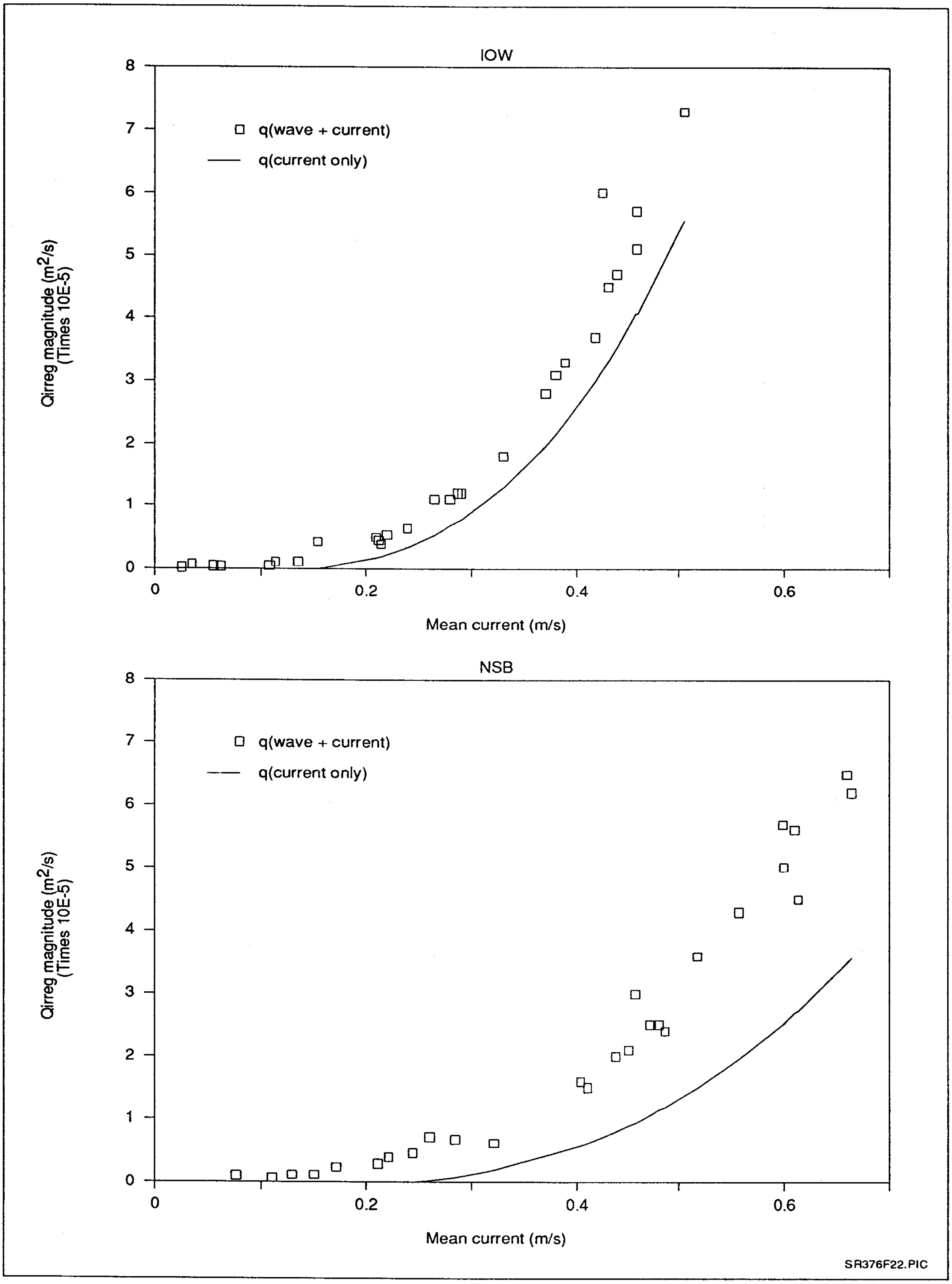

Figure 22 Magnitude of mean sediment transport (wave plus current and current only) against mean current for IOW and NSB

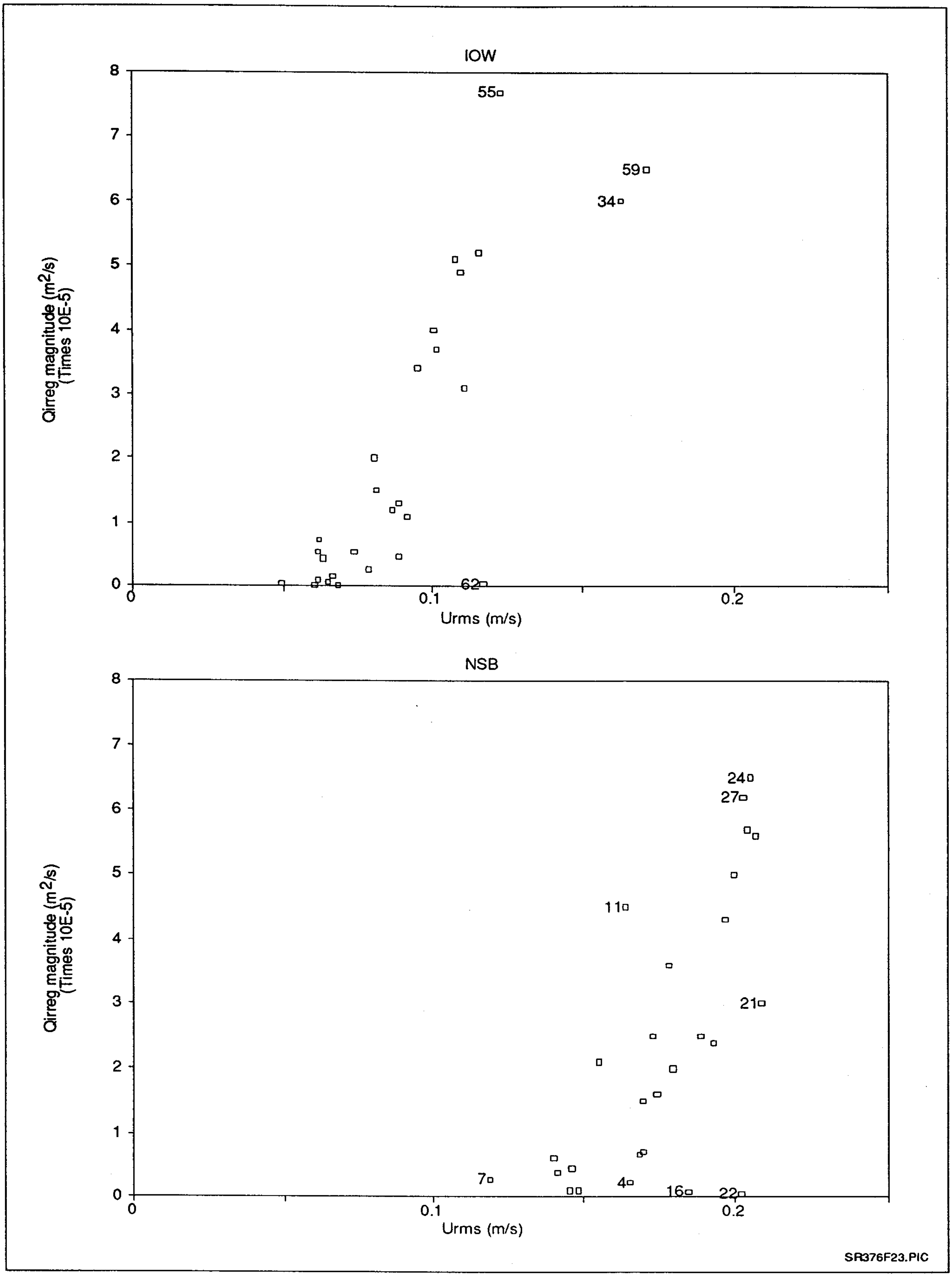

Figure 23 Magnitude of mean sediment transport (irregular) against wave orbital velocity for Isle of Wight and Norfolk Sand Banks

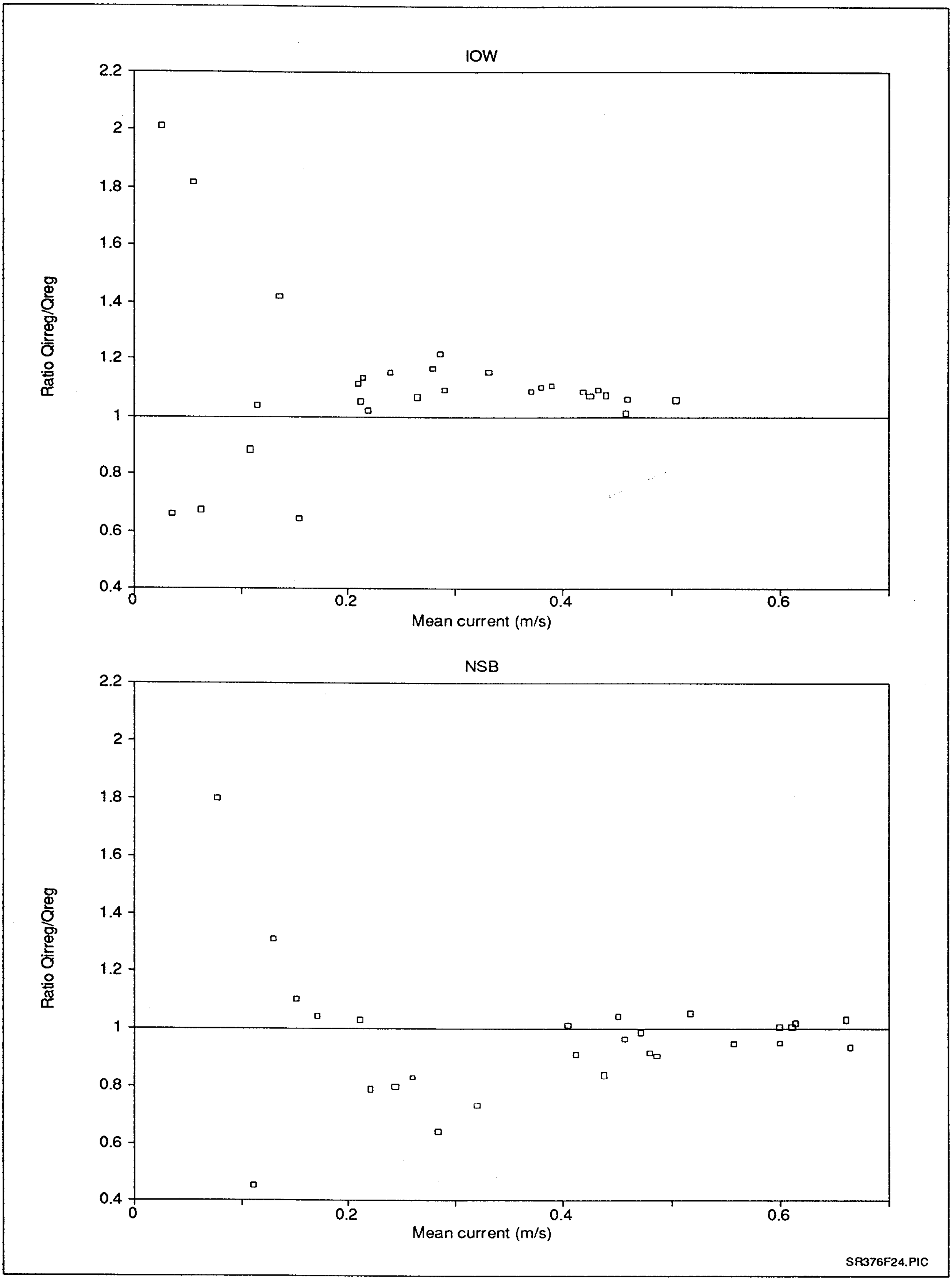

Figure 24 Ratio of mean sediment transport (irregular/regular) against mean current for Isle of Wight and Norfolk Sand Banks

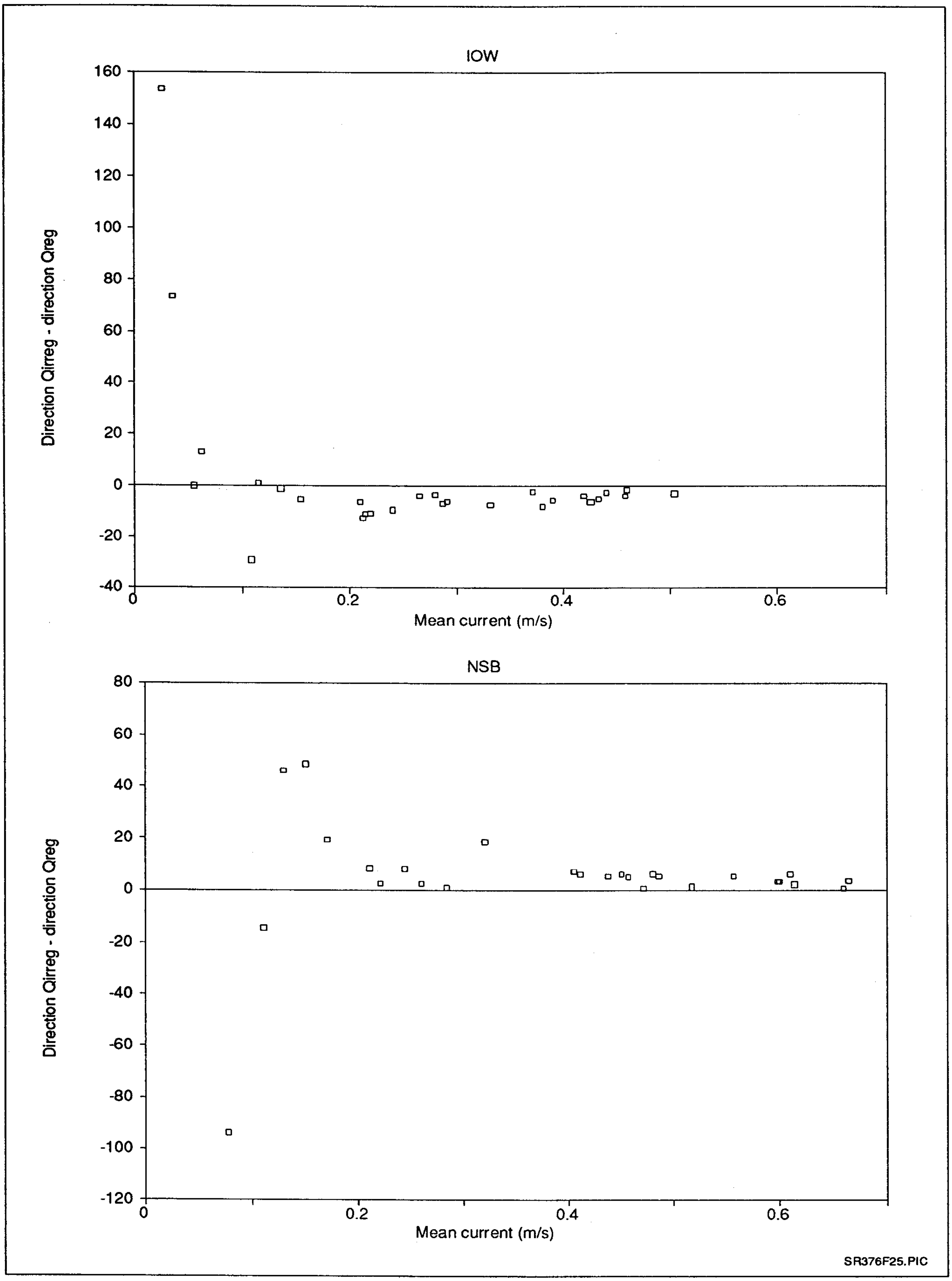

Figure 25 Difference in direction between mean transport (irregular) and mean transport (regular) against mean current for IOW and NSB

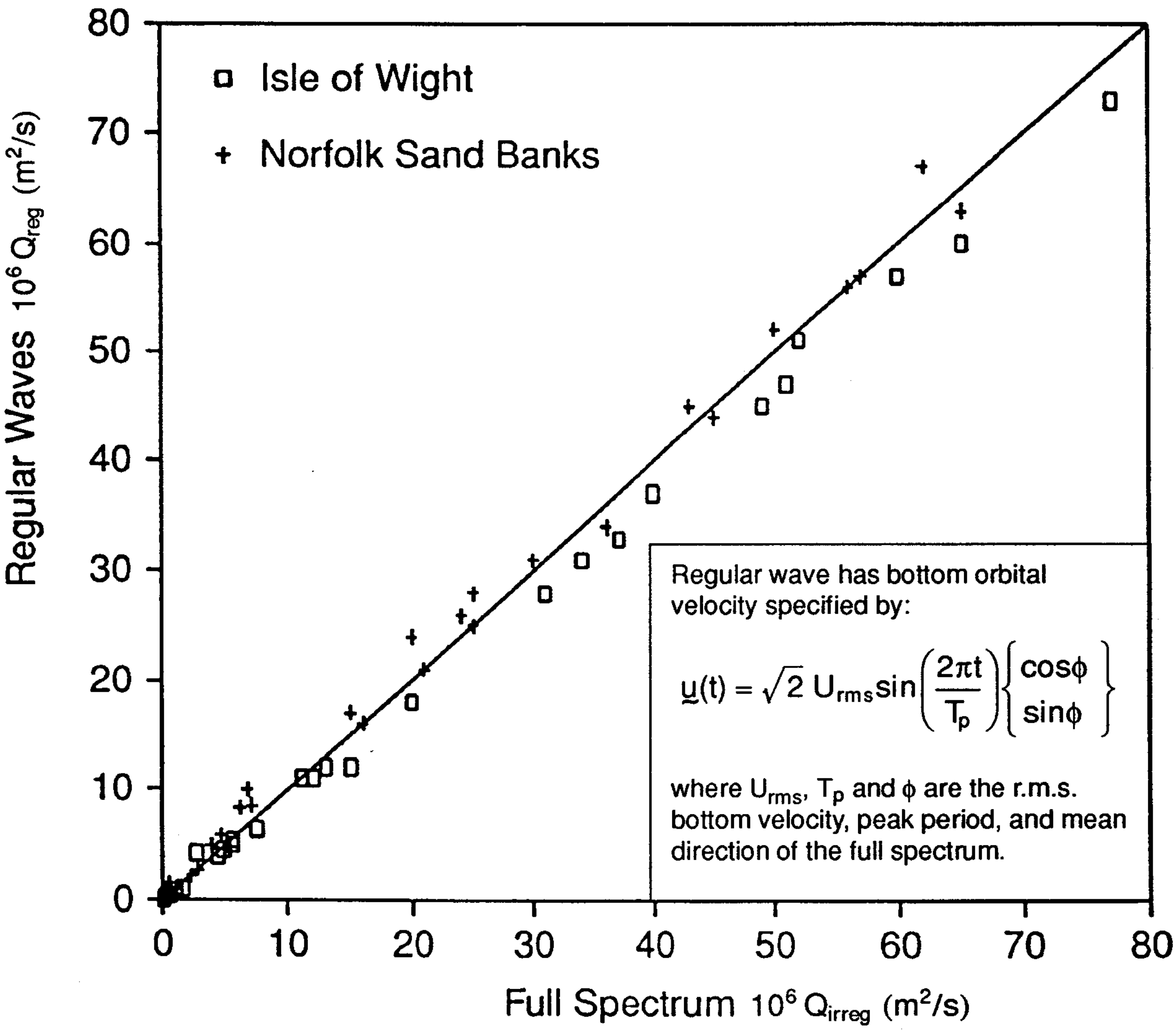

Figure 26 Comparison of sediment transport rates computed for full spectrum of waves with that for equivalent regular waves, coupled with a current

Appendix

Appendix 1

Calculation of time series of shear stress using parameterised models

Appendix 1 Calculation of time series of shear stress using parameterised models

1. Calculate current drag coefficient, C_D, applicable to the time-mean velocity $\bar{U}$, at height z_m according to

$$C_D = \left[\frac{\kappa}{\ln\left(\frac{z_m}{z_0}\right)}\right]^2$$

where

κ = von Karman's constant (0.40)
z_0= bed roughness length

2. Calculate current induced shear stress, τ_c, using:

$$\tau_c = \rho C_D \bar{U}^2$$

where

ρ = water density

3. Calculate wave friction factor, f_w, using:

$$f_w = 1.39\left(\frac{A}{z_0}\right)^{-0.52}$$

where

A is the wave excursion amplitude of a regular wave with orbital velocity = $\sqrt{2}\ U_{rms}$ and period T_p; ie

$$A = \frac{\sqrt{2}U_{rms}T_p}{2\pi}$$

with

U_{rms} = root-mean-square of orbital velocities
T_p = wave period at peak of spectrum

4. Calculate the wave-induced shear-stress amplitude, τ_w, using:

$$\tau_w = \frac{1}{2}\rho f_w W^2$$

where

W is the maximum orbital velocity of a regular wave with the same root-mean-square velocity as the irregular wave spectrum:

$$W = \sqrt{2}\,U_{rms}$$

5. Calculate the relative wave-current strength, x, according to

$$x = \frac{\tau_c}{\tau_c + \tau_w}$$

6. Calculate the theoretical mean and maximum shear stresses for a regular wave according to the parameterised boundary layer models (Soulsby et al, 1993):

$$\tau_m = (\tau_c + \tau_w)\, x\, (1 + b x^{p} (1 - x)^{q})$$

and

$$\tau_{max} = (\tau_c + \tau_w)(1 + a x^{m} (1 - x)^{n})$$

where

a, m, n, b, p, q are coefficients calculated from one of the parameterised models (user's choice).

7. Deduce an enhanced drag coefficient, C_{D+}, from

$$C_{D+} = \frac{\tau_m}{\rho \bar{U}^2}$$

8. Given the mean angle of the waves relative to the current, ϕ, deduce the enhanced wave induced shear stress, τ_{w+}, from the model, according to a vector subtraction (and assuming that the wave induced shear stress acts in the same direction as the mean direction of the waves). ie

$$\underset{\sim}{\tau}_{w+} = \underset{\sim}{\tau}_{max} - \underset{\sim}{\tau}_{m}$$

or

$$|\underset{\sim}{\tau}_{w+}| = (\tau_{max}^2 - \tau_m^2 \sin^2\phi)^{\frac{1}{2}} - \tau_m \cos\phi$$

9. Calculate an enhanced wave friction factor, f_{w+}, from

$$f_{w+} = \frac{|\underset{\sim}{\tau}_{w+}|}{0.5\rho W^2}$$

10. Calculate the instantaneous shear stress vector at each point of the time series as:

$$\underset{\sim}{\tau}(t) = \rho C_{D+}|\overline{\underset{\sim}{U}}|\,\overline{\underset{\sim}{U}} + \frac{1}{2}\rho f_{w+}\,|\underset{\sim}{u}(t)|\,\underset{\sim}{u}(t)$$

where

$\overline{\underset{\sim}{U}}$ is the time-mean velocity vector at height z_m

$\underset{\sim}{u}(t)$ is the wave-induced fluctuation in the velocity vector at height z_m about the value $\overline{\underset{\sim}{U}}$.

Note that this method ignores the phase shift between $\underset{\sim}{\tau}(t)$ and $\underset{\sim}{u}(t)$ which is observed in practice.